

# Higher-order Exceptional Points Induced by Non-Markovian Environments

H. Z. Shen<sup>1</sup>, \* X. C. Zhang<sup>1</sup>, L. Y. Ning<sup>1</sup>, Zhi-Guang Lu<sup>2</sup>, and Cheng Shang<sup>3,4†</sup>

<sup>1</sup>Center for Quantum Sciences and School of Physics,  
Northeast Normal University, Changchun 130024, China

<sup>2</sup>School of Physics, Huazhong University of Science and Technology, Wuhan, 430074, People's Republic of China

<sup>3</sup>Analytical Quantum Complexity RIKEN Hakubi Research Team,

RIKEN Center for Quantum Computing (RQC), Wako, Saitama 351-0198, Japan

<sup>4</sup>Department of Physics, The University of Tokyo, 5-1-5 Kashiwanoha, Kashiwa, Chiba 277-8574, Japan

Exceptional points (EPs) are central to non-Hermitian physics because of their unique properties and broad application prospects. While extensively studied in parity-time ( $\mathcal{PT}$ )-symmetric systems and under Markovian dynamics, their exploration in broader pseudo-Hermitian settings particularly those involving non-Markovian environments remains largely unexplored. In this study, we investigate a pseudo-Hermitian system consisting of three coupled optical cavities interacting with non-Markovian environments. Compared to the Markovian baseline, we demonstrate that the emergence of non-Markovian memory effects enlarges the dimensionality of the parameter space of the system, thereby giving rise to higher-order EPs. Moreover, we observe that the pseudo-Hermitian system with an effective gain induced by coherent perfect absorption enables the higher-order EPs to be directly read out from the output spectrum. Additionally, we find that breaking the symmetry of the parameter space of the system reduces the order of the EPs. Possible experimental implementations based on a superconducting circuit are also discussed. Our findings reveal how non-Markovianity enhances the sensitivity of the system and provide a theoretical insight into the experimental observation of higher-order EPs.

## I. INTRODUCTION

Superconducting (SC) circuits have emerged as a promising platform for quantum information processing and for investigating unique physical phenomena, as extensively reviewed in Refs. [1]. Quijandría *et al.* introduced the concept of a parity-time ( $\mathcal{PT}$ )-symmetric phase transition occurring at the exceptional point (EP) in SC circuits [2], which was subsequently observed on SC quantum computing platform of IBM by Dogra *et al.* [3]. Following these theoretical advances, a series of experiments have verified EP-related phenomena in SC platforms, with EP signatures detected in dissipative SC qubits [4–6] and in interconnected systems comprising two dissipative SC resonators [7]. Moreover, Han *et al.* have experimentally demonstrated the exceptional entanglement transition in the vicinity of an EP [8], alongside the topological invariant associated with EP3 [9], through meticulous monitoring of the dynamical behavior within SC circuits. Building on this progress, recent work by Zhang *et al.* has further advanced the field by studying the higher-order exceptional surface in SC circuits [10].

Over the past decades, exceptional points (EPs) have attracted remarkable attention [11–17]. In particular, a  $k$ th-order exceptional point (EP $k$ , with  $k \geq 2$ ) refers to a spectral singularity of a non-Hermitian Hamiltonian where  $k$  eigenvalues and their corresponding eigenstates coalesce [18–23]. In non-Hermitian systems, the spectral anomaly associated with EPs has been demonstrated to induce a multitude of fascinating phenomena, including unidirectional invisibility [24, 25], resilient wireless energy transmission [26, 27], asymmetric modal transitions [28, 29], augmented spontaneous radiation [30], unidirectional lasing [31], exotic topological

states [32], sensitivity enhancement [33–37], laser mode selection [38, 39], coherent perfect absorption [40–42], electromagnetically induced transparency [43], the speeding up of entanglement generation [44], and the exhibition of complex topological characteristics in interconnected acoustic resonators [45].

While closed quantum systems satisfy Hermiticity and thus have real spectra, practical systems are inevitably open and are effectively described by non-Hermitian Hamiltonians that typically yield complex spectra. Nevertheless, the reality of eigenvalues does not require Hermiticity; in other words, Hermiticity is not a necessary condition for a spectrum to be real. In this sense, Mostafazadeh identified a class of quantum systems exhibiting the above energy spectral properties, whose Hamiltonians are related to their adjoints through a similarity transformation  $\eta$  as in  $H = \eta^{-1}H^\dagger\eta$ , known as pseudo-Hermitian Hamiltonians [46–48], where eigenvalues are constrained to be either purely real or to appear in complex-conjugate pairs. Nowadays, systems possessing pseudo-Hermiticity have led to a wealth of interesting phenomena across diverse areas of physics, including quantum chaos, quantum phase transitions [49–51] and dynamical invariants [52].

In particular, the Hermitian Hamiltonians form a subset of pseudo-Hermitian ones, while  $\mathcal{PT}$ -symmetric Hamiltonians constitute another prominent subclass within the pseudo-Hermitian landscape [48, 53]. A quantum phase transition occurs as system parameters approach the EP, driving the system from a  $\mathcal{PT}$ -symmetric to a symmetry-broken phase. This transition is characterized by the spectrum shifting from real to complex eigenvalues [53], with the critical point termed an EP2, which has been extensively investigated in various non-Hermitian systems, including optomechanical setups [29, 54], coupled waveguides [28], optical microresonator networks [55], cavity magnonics systems [56], and superconducting circuit-QED configurations [2]. While  $\mathcal{PT}$  symme-

\* Contact author: shenzh458@nenu.edu.cn

† Contact author: cheng.shang@riken.jp

try has provided a fertile ground for exploring EPs, its stringent parameter constraints—especially in realizing higher-order EPs—motivate turning to the broader framework of pseudo-Hermiticity, which encompasses both Hermitian and  $\mathcal{PT}$ -symmetric cases yet extends beyond them to enable a wider range of non-Hermitian phenomena. In the broader pseudo-Hermitian framework without  $\mathcal{PT}$  symmetry, higher-order EPs and their applications have been widely investigated in diverse platforms, including cavity-magnon systems [57–59], cavity optomechanical systems [60, 61], radio-frequency circuits [62].

The rapid advances in quantum information technology [63] have brought open quantum systems [64–71] into sharp focus. The Markovian approximation for open quantum systems [64, 72–75] applies only in the regime of weak system–environment coupling, where the characteristic timescales of systems are significantly exceeding those of the environment. In contrast, many scenarios demand a full consideration of non-Markovian dynamics [76], which arise in diverse quantum setups such as interconnected cavities [77], photonic crystals [78], colored-noise environments [79], cavity–waveguide hybrids [66, 80–82], etc [83–99]. Such non-Markovian processes have proven crucial for a variety of quantum information tasks, including state engineering and quantum control [100, 101]. Their hallmark is the appearance of memory effects, wherein the influence of an environment on system dynamics reaches back to affect earlier states. Physically, this is often manifested as the repeated exchange of excitations between the system and its surroundings [65, 102], which in turn forms the foundation for a variety of approaches to quantifying non-Markovianity [103–108].

The primary contribution of this work is to demonstrate that non-Markovianity induces high-order EPs in a pseudo-Hermitian system comprised of three coupled optical cavities with non-Markovian environments, and further clarify the underlying physical mechanisms involved. Moreover, we highlight that these EPs can be experimentally observed through the total output spectrum using coherent perfect absorption. As a baseline, under the Markovian approximation [109–116], the effective Hamiltonian exhibits EP2 and EP3, which correspond to the asymmetric and symmetric parameter settings, respectively. Our study demonstrates that, for the three-mode system under consideration, varying the number and types of non-Markovian structured reservoirs coupled to the optical modes leads to EPs of different orders, ranging from EP4 [117–126] and EP5 [127–129] to EP6 [130, 131] and EP7. We also briefly discuss the experimental feasibility of observing higher-order EPs in a superconducting circuit [7, 132–138]. Our work lays a solid foundation for exploring the spectral structures of higher-order EPs induced by non-Markovian environments and for investigating their potential applications near the EPs, such as highly sensitive sensors [139–148].

The present paper is organized as follows. In Sec. II, we introduce our model and its non-Markovian effective Hamiltonian. In Sec. III, we demonstrate and classify higher-order EPs, elucidating the mechanism by which non-Markovian environments induce them. Possible experimental implemen-

tations are discussed in Sec. IV. Finally, we summarize the results and conclude the paper in Sec. V.

## II. MODEL AND HAMILTONIAN

Since physical systems are inevitably open, non-Markovian effects are broadly relevant. While Markovian processes can effectively capture many quantum phenomena, this approximation fails when the system strongly interacts with the environment and the environment memory time is comparable to the system characteristic time [68–70], at which point non-Markovian effects dominate. We start this section by describing our model and its governing dynamics in Sec. II A. Subsequently, we present the effective Hamiltonian and the conditions for coherent perfect absorption in Sec. II B.

### A. Model and non-Markovian dynamics

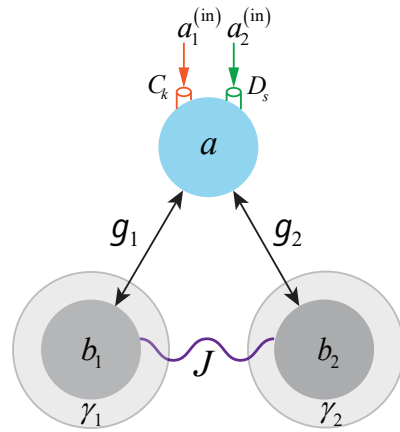


FIG. 1. Schematic of a three-mode optical cavity coupling setup in an open quantum system [139–148]. Cavity mode  $a$  couples to cavity modes  $b_1$  and  $b_2$  with strengths  $g_1$  and  $g_2$ , respectively. On the other hand, cavity modes  $b_1$  and  $b_2$  are coupled with strength  $J$ . In addition, the input fields  $a_1^{(in)}$  and  $a_2^{(in)}$  generate non-Markovian baths, which couples to cavity mode  $a$  through two ports with strengths  $C_k$  and  $D_s$ , respectively. Furthermore, cavity modes  $b_1$  and  $b_2$  are each coupled to Markovian environments with dissipation rates  $\gamma_1$  and  $\gamma_2$ .

*Model.* We consider a three-mode optical open quantum system as illustrated in Fig. 1. The central cavity mode  $a$  couples to two side cavities  $b_1$  and  $b_2$  with interaction strengths  $g_1$  and  $g_2$ , respectively, while the two side cavities are coupled to each other with strength  $J$ . Moreover, cavity  $a$  is driven by two input fields  $a_1^{(in)}$  and  $a_2^{(in)}$  through two ports, which are equivalent to being coupled to two structured non-Markovian reservoirs, each consisting of a series of bosonic modes  $c_k$  and  $d_k$ , with coupling strengths  $C_k$  and  $D_s$ , respectively. On the other hand, the side cavities  $b_1$  and  $b_2$  interact with their respective Markovian reservoirs, characterized phenomenologically by dissipation rates  $\gamma_1$  and  $\gamma_2$ . We assume that the two input fields have the same frequency  $\omega_p$ . In the rotating frame

with  $\omega_p$ , the total Hamiltonian can be written as

$$H_T = H_S + H_E, \quad (1)$$

where

$$H_S = \Delta_a a^\dagger a + \Delta_{b_1} b_1^\dagger b_1 + \Delta_{b_2} b_2^\dagger b_2 + g_1 (a^\dagger b_1 + a b_1^\dagger) + g_2 (a^\dagger b_2 + a b_2^\dagger) + J (b_1^\dagger b_2 + b_1 b_2^\dagger), \quad (2)$$

$$H_E = \sum_k \Omega_k c_k^\dagger c_k + i \sum_k (C_k a c_k^\dagger - C_k^* a^\dagger c_k) + \sum_s \varpi_s d_s^\dagger d_s + i \sum_s (D_s a d_s^\dagger - D_s^* a^\dagger d_s), \quad (3)$$

where  $a$  ( $a^\dagger$ ) denotes the annihilation (creation) operator of cavity  $a$  with eigenfrequency  $\omega_a$ , while  $b_1$  ( $b_1^\dagger$ ) and  $b_2$  ( $b_2^\dagger$ ) denote those of cavity  $b_1$  and  $b_2$  with eigenfrequency  $\omega_{b_1}$  and  $\omega_{b_2}$ . Additionally,  $\nu_k$  and  $\mu_s$  correspond to the eigenfrequencies of the environmental modes  $c_k$  and  $d_s$ , respectively. Within the rotating frame, the frequency detunings are denoted as  $\Delta_a = \omega_a - \omega_p$ ,  $\Delta_{b_1} = \omega_{b_1} - \omega_p$ ,  $\Delta_{b_2} = \omega_{b_2} - \omega_p$ ,  $\Omega_k = \nu_k - \omega_p$ , and  $\varpi_s = \mu_s - \omega_p$ .

*Dynamics and the non-Markovian input–output relation.* For Hamiltonian (1), the corresponding Heisenberg equations are given by

$$\begin{aligned} \dot{a} &= -i\Delta_a a - ig_1 b_1 - ig_2 b_2 - \sum_k C_k^* c_k - \sum_s D_s^* d_s, \\ \dot{b}_1 &= -i(\Delta_{b_1} - i\gamma_1) b_1 - ig_1 a - iJ b_2, \\ \dot{b}_2 &= -i(\Delta_{b_2} - i\gamma_2) b_2 - ig_2 a - iJ b_1, \\ \dot{c}_k &= -i\Omega_k c_k + C_k a, \quad \dot{d}_s = -i\varpi_s d_s + D_s a. \end{aligned} \quad (4)$$

Solving Eq. (4) yields the time-dependent environment operators for  $t \geq 0$  in the form:

$$\begin{aligned} c_k(t) &= c_k(0) e^{-i\Omega_k t} + C_k \int_0^t d\tau a(\tau) e^{-i\Omega_k(t-\tau)}, \\ d_s(t) &= d_s(0) e^{-i\varpi_s t} + D_s \int_0^t d\tau a(\tau) e^{-i\varpi_s(t-\tau)}, \end{aligned} \quad (5)$$

which can be divided into two components. The first term in  $c_k(t)$  or  $d_s(t)$  corresponds to the evolution of the non-Markovian environmental field, while the second term reflects the feedback of non-Markovian effects from the environment to cavity  $a$ . Further, substituting Eq. (5) into Eq. (4) yields the integro-differential equation for the cavity operator

$$\begin{aligned} \dot{a} &= -i\Delta_a a - ig_1 b_1 - ig_2 b_2 + K_1 + K_2 \\ &\quad - \int_0^t d\tau a(\tau) [f_1(t-\tau) + f_2(t-\tau)], \end{aligned} \quad (6)$$

where  $K_1 = -\sum_k C_k^* c_k(0) e^{-i\Omega_k t} = \int_{-\infty}^{\infty} d\tau \kappa_1^*(t-\tau) a_1^{(in)}(\tau)$ ,  $K_2 = -\sum_s D_s^* d_s(0) e^{-i\varpi_s t} = \int_{-\infty}^{\infty} d\tau \kappa_2^*(t-\tau) a_2^{(in)}(\tau)$ . Herein, the input field operators are defined as  $a_1^{(in)}(t) = -1/\sqrt{2\pi} (\sum_k c_k(0) e^{-i\Omega_k t})$ ,  $a_2^{(in)}(t) = -1/\sqrt{2\pi} (\sum_s d_s(0) e^{-i\varpi_s t})$ , and the impulse response functions in the continuum limit are denoted by

$$\kappa_1(t-\tau) = \frac{1}{\sqrt{2\pi}} \int_{-\infty}^{+\infty} d\omega e^{i\omega(t-\tau)} C(\omega),$$

$$\kappa_2(t-\tau) = \frac{1}{\sqrt{2\pi}} \int_{-\infty}^{+\infty} d\omega' e^{i\omega'(t-\tau)} D(\omega'), \quad (7)$$

where  $C_k \rightarrow C(\omega)$  and  $D_s \rightarrow D(\omega')$ . Notably, the correlation functions  $f_1(t)$  and  $f_2(t)$  in Eq. (6) play a central role by acting as memory kernels, which are given by

$$\begin{aligned} f_1(t) &= \int_{-\infty}^{+\infty} S_1(\omega) e^{-i\omega t} d\omega, \\ f_2(t) &= \int_{-\infty}^{+\infty} S_2(\omega') e^{-i\omega' t} d\omega', \end{aligned} \quad (8)$$

where  $S_1(\omega) = |C(\omega)|^2$  and  $S_2(\omega') = |D(\omega')|^2$  are referred to as the spectral densities of the reservoirs. Similarly, for  $0 \leq t \leq t_1$ , the solution for the output field operator reads

$$\begin{aligned} a_1^{(out)}(t) &= \frac{1}{\sqrt{2\pi}} \sum_k c_k(t_1) e^{-i\Omega_k(t-t_1)}, \\ a_2^{(out)}(t) &= \frac{1}{\sqrt{2\pi}} \sum_s d_s(t_1) e^{-i\varpi_s(t-t_1)}. \end{aligned} \quad (9)$$

Combining Eq. (6) to Eq. (9) and taking the limit  $t_1 \rightarrow t$ , we obtain the non-Markovian input–output relation for the port of cavity  $a$  as follows:

$$a_{1(2)}^{(in)}(t) + a_{1(2)}^{(out)}(t) = \int_0^t \kappa_{1(2)}(\tau-t) a(\tau) d\tau. \quad (10)$$

Taking the impulse response functions given in Eq. (7) as  $\kappa_1(t) = \lambda_1 \sqrt{\Gamma_1} e^{\lambda_1 t} \vartheta(-t)$  and  $\kappa_2(t) = \lambda_2 \sqrt{\Gamma_2} e^{\lambda_2 t} \vartheta(-t)$ , we obtain the correlation functions  $f_1(t) = \lambda_1 \Gamma_1 e^{-\lambda_1 |t|}/2$  and  $f_2(t) = \lambda_2 \Gamma_2 e^{-\lambda_2 |t|}/2$  from Eq. (8), where  $\vartheta(-t)$  is the step function, defined as  $\vartheta(-t) = 1$  for  $t \leq 0$  and  $\vartheta(-t) = 0$  for  $t > 0$ . After Fourier transform to Eq. (7), the corresponding spectral response functions read  $C(\omega) = \sqrt{\Gamma_1/2\pi} [\lambda_1/(\lambda_1 - i\omega)]$  and  $D(\omega') = \sqrt{\Gamma_2/2\pi} \lambda_2/[(\lambda_2 - i\omega')]$ , where  $\lambda_1$  and  $\lambda_2$  represent the spectral widths of the two non-Markovian environments, while  $\Gamma_1$  and  $\Gamma_2$  denote the cavity dissipation rates coupled to the two ports. Consequently, the Lorentzian spectral densities [149] are given by

$$S_1(\omega) = \frac{\Gamma_1}{2\pi} \frac{\lambda_1^2}{\lambda_1^2 + \omega^2}, \quad S_2(\omega') = \frac{\Gamma_2}{2\pi} \frac{\lambda_2^2}{\lambda_2^2 + (\omega')^2}, \quad (11)$$

which characterize a Gaussian Ornstein–Uhlenbeck process [150].

Intuitively, the memory effect associated with non-Markovian reservoirs disappears as the spectral width  $\lambda_1$  and  $\lambda_2$  approach infinity, leading to a return to the case [151, 152]. Notably, the above derivation can also be carried out using the pseudomode theory, with details provided in Appendix A.

## B. CPA condition and non-Markovian effective Hamiltonian

For simplicity, let us consider the case where the two non-Markovian environments provided by the two ports are identical, i.e., the non-Markovian environmental spectral widths

and the cavity dissipation rates coupled to the two ports respectively satisfy  $\lambda_1 = \lambda_2 \equiv \lambda$  and  $\Gamma_1 = \Gamma_2 \equiv \Gamma$ . The general case of two different non-Markovian environments provided by the two ports is discussed in Appendix B.

In the simple case, combining Eq. (6) with Eq. (4) yields

$$\begin{aligned}\dot{a} &= -i\Delta_a a - ig_1 b_1 - ig_2 b_2 + K_1 + K_2 \\ &\quad - \int_0^t d\tau a(\tau) [f_1(t-\tau) + f_2(t-\tau)], \\ \dot{b}_1 &= -i(\Delta_{b_1} - i\gamma_1)b_1 - ig_1 a - iJb_2, \\ \dot{b}_2 &= -i(\Delta_{b_2} - i\gamma_2)b_2 - ig_2 a - iJb_1.\end{aligned}\quad (12)$$

*The CPA condition.* For suitably chosen parameters, coherent perfect absorption (CPA) occurs when the output fields vanish,  $a_1^{(\text{out})}(t) = a_2^{(\text{out})}(t) = 0$ . The system exhibits an effective gain through the CPA of the two input fields at port  $a$ , allowing the Hamiltonian to be pseudo-Hermitian, which can be identified by analyzing the total output spectrum (see Sec. III A).

To analyze the CPA condition, we perform a modified Laplace transform [153, 154] on Eq. (12) and obtain (derivation details can be found in Appendix C)

$$\begin{aligned}-i\omega a(\omega) &= -[i\Delta_a + f_1(\omega) + f_2(\omega)]a(\omega) - ig_1 b_1(\omega) \\ &\quad - ig_2 b_2(\omega) + \tilde{\kappa}_1(\omega)a_1^{(\text{in})}(\omega) + \tilde{\kappa}_2(\omega)a_2^{(\text{in})}(\omega), \\ -i\omega b_1(\omega) &= -i(\Delta_{b_1} - i\gamma_1)b_1(\omega) - ig_1 a(\omega) - iJb_2(\omega), \\ -i\omega b_2(\omega) &= -i(\Delta_{b_2} - i\gamma_2)b_2(\omega) - ig_2 a(\omega) - iJb_1(\omega),\end{aligned}\quad (13)$$

where we have  $f_{1(2)}(\omega) = \int_0^\infty f_{1(2)}^*(t')e^{i\omega t'}dt'$ ,  $\tilde{\kappa}_{1(2)}(\omega) = \int_{-\infty}^0 \kappa_{1(2)}^*(t')e^{i\omega t'}dt'$ , and  $a_{1(2)}^{(\text{in})}(\omega) = \int_0^\infty a_{1(2)}^{(\text{in})}(t')e^{i\omega t'}dt'$ . Then, the cavity field  $a(\omega)$  follows directly from Eq. (13) and is given by

$$a(\omega) = \frac{\tilde{\kappa}_1(\omega)a_1^{(\text{in})}(\omega) + \tilde{\kappa}_2(\omega)a_2^{(\text{in})}(\omega)}{f_1(\omega) + f_2(\omega) + i(\Delta_a - \omega) + \sigma(\omega)}, \quad (14)$$

where  $\sigma(\omega) = (ig_1^2\Theta_2 + ig_2^2\Theta_1 + 2ig_1g_2J)/(J^2 - \Theta_1\Theta_2)$  denote the self-energy of cavities  $b_1$  and  $b_2$  with  $\Theta_{1(2)} = (\omega_{b_{1(2)}} - \omega) - i\gamma_{1(2)}$ . Furthermore, the non-Markovian input-output relation (10) in the frequency domain reads

$$a_{1(2)}^{(\text{in})}(\omega) + a_{1(2)}^{(\text{out})}(\omega) = a(\omega)\kappa_{1(2)}(-\omega). \quad (15)$$

The CPA occurs when the following two conditions are satisfied simultaneously, as obtained by substituting Eq. (14) into Eq. (15) with  $a_{1(2)}^{(\text{out})}(\omega_{\text{CPA}}) = 0$ , then we have

$$\frac{a_1^{(\text{in})}(\omega_{\text{CPA}})}{a_2^{(\text{in})}(\omega_{\text{CPA}})} = \frac{\kappa_1(-\omega_{\text{CPA}})}{\kappa_2(-\omega_{\text{CPA}})} \quad (16)$$

and

$$\begin{aligned}\omega_{\text{CPA}} &= i[\tilde{\kappa}_1(\omega_{\text{CPA}})\kappa_1(-\omega_{\text{CPA}}) + \tilde{\kappa}_2(\omega_{\text{CPA}})\kappa_2(-\omega_{\text{CPA}})] \\ &\quad - i[f_1(\omega_{\text{CPA}}) + f_2(\omega_{\text{CPA}}) + \sigma(\omega_{\text{CPA}})] + \Delta_a,\end{aligned}\quad (17)$$

where  $\omega_{\text{CPA}}$  represents the frequency of the input fields at which CPA occurs, and  $\sigma(\omega_{\text{CPA}})$  is obtained from  $\sigma(\omega)$ .

Conditions (16) and (17) indicate that the occurrence of CPA depends on both the tuning of system parameters and choosing appropriate input fields, where the two input fields must share the same phase and maintain an amplitude ratio of  $\kappa_1(-\omega_{\text{CPA}})/\kappa_2(-\omega_{\text{CPA}})$ , which can be realized experimentally by using a tunable phase shifter and a variable attenuator [41].

*Effective Hamiltonian and pseudo-Hermiticity.* In the CPA regime, Eq. (10) reduces to  $a_{1(2)}^{(\text{in})}(t) = \int_0^t \kappa_{1(2)}(\tau-t)a(\tau)d\tau$ . By taking this into account and defining  $2gX(t) := K_1^\dagger(t) + K_2^\dagger(t) - \int_0^t d\tau a(\tau) [f_1(t-\tau) + f_2(t-\tau)]$  with  $g = \sqrt{\lambda\Gamma/2}$ , Eq. (12) becomes  $\dot{\mathbf{V}} = -iH_{\text{eff}}\mathbf{V}$ , where  $\mathbf{V} = (a, b_1, b_2, X)^T$  and the effective non-Markovian Hamiltonian  $H_{\text{eff}}$  can be expressed as

$$H_{\text{eff}} = \begin{pmatrix} \Delta_a & g_1 & g_2 & -2ig \\ g_1 & \Delta_{b_1} - i\gamma_1 & J & 0 \\ g_2 & J & \Delta_{b_2} - i\gamma_2 & 0 \\ ig & 0 & 0 & i\lambda \end{pmatrix}. \quad (18)$$

Next, we verify under what parameter constraints the effective Hamiltonian (18) satisfies pseudo-Hermiticity. Hamiltonian (18) has a quartet of eigenvalues. According to the method in Ref. [46],  $H_{\text{eff}}$  is pseudo-Hermitian if all four eigenvalues are real. From the spectral properties of pseudo-Hermitian Hamiltonians, this condition is equivalent to demanding that  $\det(H_{\text{eff}} - \mathbb{E}\mathbb{I}) = 0$  and its complex conjugate  $\det(H_{\text{eff}}^* - \mathbb{E}\mathbb{I}) = 0$  possess identical solutions, where  $\mathbb{I}$  denotes the identity matrix and  $\mathbb{E}$  are the eigenvalues of Eq. (18). Expanding the characteristic equation and its complex conjugate, and then comparing the corresponding coefficients, yield a set of constraints under which the effective Hamiltonian is pseudo-Hermitian, as follows

$$\begin{aligned}(g_1)^2\gamma_2 + (g_2)^2\gamma_1 - \lambda(\Delta_{b_1}\Delta_{b_2} + \lambda\Gamma - \gamma_1\gamma_2 - J^2) &= 0, \\ (g_2)^2\Delta_{b_1} + (g_1)^2\Delta_{b_2} + (J^2 + \gamma_1\gamma_2 - \Delta_{b_1}\Delta_{b_2})\Delta_a \\ - 2Jg_1g_2 - \Gamma(\gamma_2\Delta_{b_1} + \gamma_1\Delta_{b_2}) &= 0, \\ \lambda - \gamma_1 - \gamma_2 &= 0, \quad \gamma_1\Delta_{b_1} + \gamma_2\Delta_{b_2} = 0.\end{aligned}\quad (19)$$

### III. HIGHER-ORDER EXCEPTIONAL POINTS

In this section, we first present numerical results for the example discussed in Sec. II B, demonstrating that when the effective Hamiltonian satisfies pseudo-Hermiticity, the non-Markovian structured reservoir—compared with its Markovian counterpart—can induce a higher-order EP, namely EP4. We further show that EP4 can be tracked and identified from the spectral structure of the total output spectrum, and provide a detailed analysis of the transition from EP2 to EP4 in this case. Finally, moving beyond this case, we classify the possible higher-order EPs and their corresponding scenarios in a three-mode optical open system.

### A. Emergence of higher-order EPs

Without loss of generality, we continue with the simple case in Sec. II B, where the two ports of cavity  $a$  are coupled to identical non-Markovian structured reservoirs. By deriving the total output spectrum of cavity  $a$  coupled to a non-Markovian structured reservoir, we numerically demonstrate the pseudo-Hermiticity of the system and further show that higher-order EPs can be read out through spectral analysis.

Under condition (16), Eq. (15) can be rewritten in the form  $a_{1(2)}^{(\text{out})}(\omega) = T_{1(2)}(\omega) a_{1(2)}^{(\text{in})}(\omega)$ , where  $T_{1(2)}(\omega)$  is the scattering matrix at port 1 or 2, and its corresponding scattering probability is given by  $|T_{1(2)}(\omega)|^2$ . Explicitly,  $T_1$  and  $T_2$  are expressed as

$$T_1(\omega) = \frac{\kappa_1(-\omega)\tilde{\kappa}_1(\omega) + \kappa_2(-\omega)\tilde{\kappa}_2(\omega)}{f_1(\omega) + f_2(\omega) + i(\Delta_a - \omega) + \sigma(\omega)} - 1 \quad (20)$$

and  $T_1(\omega) = T_2(\omega)$ . To further describe the input-output characteristics of the whole system, we introduce the total output spectral function of cavity  $a$ , denoted as

$$|T_{\text{tot}}(\omega)|^2 = |T_1(\omega)|^2 + |T_2(\omega)|^2 = 2|T_1(\omega)|^2. \quad (21)$$

We note that once the remaining necessary condition (17) for CPA is also satisfied, the total output spectrum  $|T_{\text{tot}}(\omega_{\text{CPA}})|^2$  becomes zero.

We now verify the pseudo-Hermiticity of the system and numerically observe the emergence of an EP4 through the total output spectrum in a simple case. Specifically, we set equal coupling strengths,  $g_1 = g_2$ , between cavities  $b_1$ ,  $b_2$ , and  $a$ , and further consider two cases where the dissipation of  $b_1$  and  $b_2$  are symmetric  $\gamma_1 = \gamma_2$  and asymmetric  $\gamma_1 \neq \gamma_2$ .

First, we present the parameter conditions required for the system to satisfy pseudo-Hermiticity in the numerical simulations. For the symmetric case, the pseudo-Hermiticity condition of the system in Eq. (19) reads  $\lambda = 2\gamma_2$ ,  $\Delta_{b_2} = -\Delta_{b_1}$ ,  $\Delta_a = 0$  and  $\Gamma = (g_1^2 + \gamma_2^2 + \Delta_{b_1}^2)/2\gamma_2$ ; while for the asymmetric case,  $\gamma_1 = 2\gamma_2$ , it becomes  $\lambda = 3\gamma_2$ ,  $\Delta_{b_2} = -2\Delta_{b_1} = 2\Delta_a$  and  $\Gamma = (2g_1^2 + 6\gamma_2^2 + 6\Delta_{b_1}^2)/9\gamma_2$ .

Then, we observe the emergence of EP4 induced by a non-Markovian reservoir. In Fig. 2(a) and Fig. 2(b), we present the total output spectrum as a function of the coupling strength  $g_1$  between cavity  $b_1$  and  $a$ , and frequency detuning  $(\omega - \Delta_a)$  between the input field and cavity  $a$ , for the symmetric and asymmetric cases, respectively. The minima in the total output spectrum, highlighted by the dark red contour, correspond to the condition of CPA. They reveal that the CPA frequency  $\omega_{\text{CPA}}$  agrees well with the real parts of the eigenvalues of the effective Hamiltonian (18) under the pseudo-Hermiticity condition (19), which are marked by the white dashed lines. The above analysis not only demonstrates the experimental potential for probing the energy spectrum structure by monitoring the total output spectrum, but also establishes the theoretical feasibility of using this approach to track and identify critical singular points, such as the EP4, in the non-Markovian system.

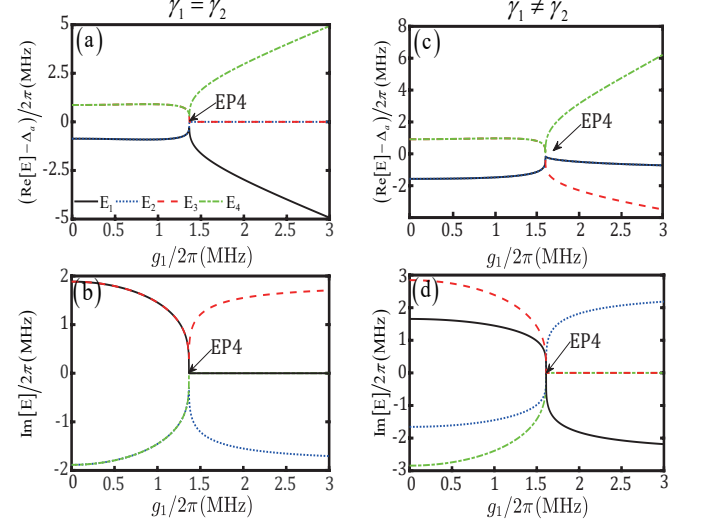


FIG. 3. The real and imaginary parts of the eigenvalues obtained from the characteristic equation (22) as functions of the coupling strength  $g_1$ . Panels (a) and (b) correspond to the symmetric case with parameters as in Fig. 2(a), whereas (c) and (d) show the asymmetric case with parameters as in Fig. 2(b).

Furthermore, we analytically determine the EP4 by directly solving the characteristic equation of the effective Hamiltonian (18) under the pseudo-Hermiticity condition (19). With  $\lambda_1 = \lambda_2 \equiv \lambda$  and  $\Gamma_1 = \Gamma_2 \equiv \Gamma$ , the characteristic equation expands to

$$x^4 + ax^3 + bx^2 + cx + d = 0, \quad (22)$$

where  $x = E - \Delta_a$ , and  $E$  is the eigenvalue of Eq. (18) under the pseudo-Hermiticity condition (19). The coefficients in Eq. (22) are explicitly given by  $a = -\Delta_{b_1} - \Delta_{b_2} + 3\Delta_a$ ,  $b = -g_1^2 - g_2^2 - J^2 - \Gamma\lambda + \lambda^2 - \gamma_1\gamma_2 + \Delta_{b_1}\Delta_{b_2} + 3\Delta_a^2 - 2(\Delta_{b_1} + \Delta_{b_2})\Delta_a$ ,  $c = 2g_2^2(\Delta_{b_1} - \Delta_a) + 2g_1^2(\Delta_{b_2} - \Delta_a) - 4Jg_1g_2 - \lambda(\gamma_2\Delta_{b_1} + \gamma_1\Delta_{b_2}) + \lambda(\lambda - 2\Gamma)\Delta_a - (\Delta_{b_1} + \Delta_{b_2})\Delta_a^2 + \Delta_a^3$ , and

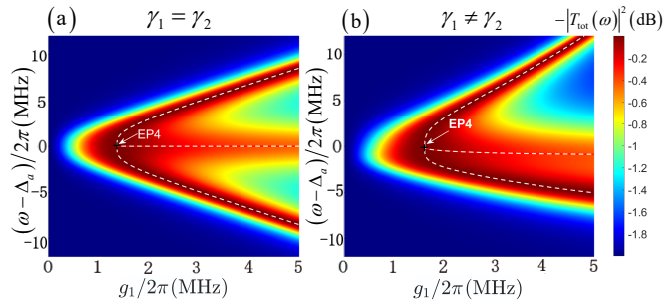


FIG. 2. The total output spectrum (21) varies with the coupling strength  $g_1$  and the frequency detuning  $(\omega - \Delta_a)$  between the input field and cavity  $a$ , for (a) symmetric and (b) asymmetric cases. The parameter settings for (a) are  $\gamma_1/2\pi = \gamma_2/2\pi = 1.885$  MHz,  $\lambda_1/2\pi = \lambda_2/2\pi = 3.77$  MHz,  $\Gamma_1/2\pi = \Gamma_2/2\pi = 1.637$  MHz,  $g_1 = g_2$ ,  $J = 0$ ,  $\Delta_{b_2} = -\Delta_{b_1}$ , and  $\Delta_a = 0$ . Parameters for (b) are chosen as  $\gamma_1/2\pi = \gamma_2/2\pi = 3$  MHz,  $\lambda_1/2\pi = \lambda_2/2\pi = 4.5$  MHz,  $\Gamma_1/2\pi = \Gamma_2/2\pi = 1.942$  MHz,  $g_1 = g_2$ ,  $J = 0$ , and  $\Delta_{b_2} = -2\Delta_{b_1} = 2\Delta_a$ .

$d = 2\Gamma(\gamma_2\Delta_{b_1} + \gamma_1\Delta_{b_2})\Delta_a - (J^2 + \Gamma\lambda + \gamma_1\gamma_2 - \Delta_{b_1}\Delta_{b_2})\Delta_a^2 - g_2^2(\lambda\gamma_1 + \Gamma\lambda_2 + \Delta_a^2) - g_1^2(\lambda\gamma_2 + \Gamma\lambda_1 + \Delta_a^2) + \Gamma^2\lambda^2$ . According to the discriminant of a quartic equation, when the condition  $B^2 - 4AC = 0$  is satisfied, the equation possesses four degenerate real roots, where  $A = D^2 - 3F$ ,  $B = DF - 9E^2$ , and  $C = F^2 - 3DE^2$ . Herein, there are  $D = 3a^2 - 8b$ ,  $E = -a^3 + 4ab - 8c$ ,  $F = 3a^4 + 16b^2 - 16a^2b + 16ac - 64d$ . When  $D = E = F = 0$ , Eq. (22) possesses a quadruple real root, i.e.,  $E_1 = E_2 = E_3 = E_4 = -a/4 = -2b/3a = -3c/2b = -4b/c$ .

Next, corresponding to Fig. 2, we present the real and imaginary parts of the eigenvalues of the system as functions of the coupling strength  $g_1$ , and further show the transition from the non-Markovian to the Markovian regime as the environmental spectral width  $\lambda$  increases.

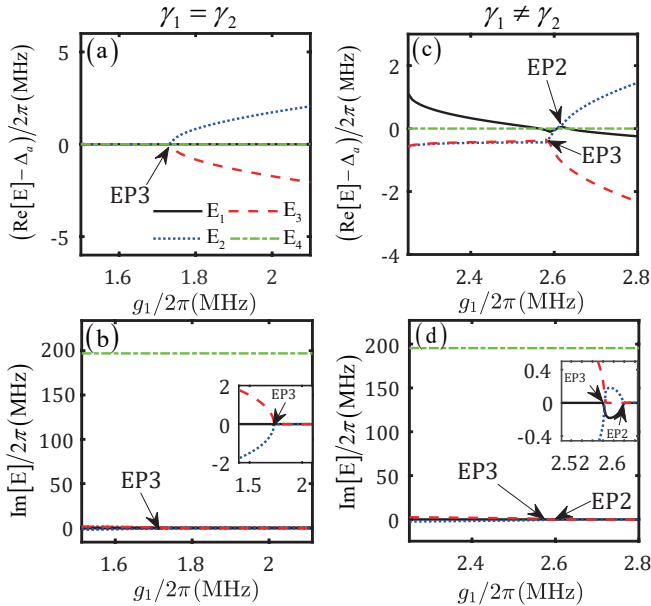


FIG. 4. The Markovian counterparts of Fig. 3. Panels (a) and (b) present symmetric cases, where the parameters are set to  $\lambda_1/2\pi = \lambda_2/2\pi = 200\text{MHz}$  and  $\Gamma_1 = \Gamma_2 = 2\gamma_1 = 2\gamma_2$ . The asymmetric case is illustrated in panels (c) and (d), with the parameter chosen as  $\lambda_1/2\pi = \lambda_2/2\pi = 200\text{MHz}$ ,  $\Gamma_1/2\pi = \Gamma_2/\pi = 4.5\text{MHz}$ , and  $\gamma_1 = 2\gamma_2$ . The remaining parameters are chosen to be the same as those in Fig. 2.

For the symmetric case  $\gamma_1 = \gamma_2$ , Fig. 3(a) and Fig. 3(b) exhibit that the critical coupling strength at EP4 is  $g_{\text{EP4}} = 1.367\text{ MHz}$ . At this point, all four eigenvalues coalesce into a single real value. Furthermore, for  $g_1 < g_{\text{EP4}}$ , the four eigenvalues appear as two complex-conjugate pairs, whereas for  $g_1 > g_{\text{EP4}}$ , the spectrum splits into two real eigenvalues and one complex-conjugate pair. In contrast, Fig. 3(c) and Fig. 3(d) present the asymmetric case:  $2\gamma_2 = \gamma_1 \neq \gamma_2$ . In this case, the critical coupling strength at the EP4 is  $g_{\text{EP4}}/2\pi = 1.610\text{ MHz}$ . Compared with Fig. 3(a), the difference is that the symmetry of the real part of eigenvalues with respect to the axis  $\text{Re}[E] = \Delta_a$  is broken. Moreover, for  $g_1 < g_{\text{EP4}}$ , the imaginary part, as shown in Fig. 3(d) compared to Fig. 3(b), displays a splitting of the two complex-conjugate pairs.

TABLE I. Symbols and their physical meanings.

Symbol	Meaning
$g_{1(2)}$	Coupling strength between cavity modes $a$ and $b_{1(2)}$
$J$	Linear coupling strength between cavities $b_1$ and $b_2$
$\gamma_{1(2)}$	Markovian dissipation rate of cavity $b_{1(2)}$
$\Gamma_{1(2)}$	Dissipation rate of cavity $a$ at port 1(2).
$\lambda_{1(2)}$	Spectral width of the non-Markovian bath at port 1(2)
$\Upsilon_{1(2)}$	Non-Markovian bath dissipation rate of cavity $b_{1(2)}$
$\Lambda_{1(2)}$	Spectral width of the non-Markovian bath of cavity $b_{1(2)}$

Finally, we examine the decay of non-Markovian effects as the spectral width of the non-Markovian environment increases, for both symmetric and asymmetric cases. For the symmetric case, we find that as the spectral width of the non-Markovian environment increases from being exceedingly narrow in Fig. 3(a) and Fig. 3(b) to being remarkably broad in Fig. 4(a) and Fig. 4(b), the non-Markovian reservoir effectively reduces to a Markovian one, and EP4 degenerates into EP3. Interestingly, when the parameter symmetry is broken in the asymmetric case, compared with the symmetric case, the transition from the non-Markovian to the Markovian shown in Fig. 4(c) and Fig. 4(d) exhibits not only the conversion from EP4 to EP3 but also that from EP4 to EP2. Additionally, the imaginary parts in Fig. 4(b) and Fig. 4(d) exhibit an additional green dashed line compared with the Markovian counterpart, corresponding to the chosen spectral width of the non-Markovian environment. Notably, the above analysis is restricted to the balanced bilateral-coupling scenario with  $g_1 = g_2$ , which leads to  $J = 0$ . For the unbalanced bilateral-coupling case with  $g_1 \neq g_2$ , resulting in  $J \neq 0$ , as well as the more general situation of broken parameter symmetry, i.e.,  $\gamma_1 \neq \gamma_2$  and  $g_1 \neq g_2$ , detailed analyses are provided in Appendix D.

## B. Classification of higher-order EPs

In the preceding discussion, we have shown that non-Markovian environments, in contrast to their Markovian counterparts, can induce higher-order EPs. However, the above analysis has focused on the simplest case, where only cavity  $a$  is coupled to a non-Markovian environment, the two structured non-Markovian reservoirs provided by the two ports are identical ( $\lambda_1 = \lambda_2$  and  $\Gamma_1 = \Gamma_2$ ), the bilateral couplings are balanced ( $g_1 = g_2$ ), and it follows that the linear coupling equals zero ( $J = 0$ ). While the analysis of the simplest case is meaningful and provides us with a clear perspective on how non-Markovian structured reservoirs induce higher-order EPs, beyond this example, we now carry out a multi-parameter exploration of the higher-order EPs that may emerge in three-mode open optical systems. In this subsection, we present only the classification results of higher-order EPs based on different scenarios and parameter conditions, while the related details and derivation can be found in Appendix E. We emphasize that classifying higher-order EPs hinges on the mem-

ory effect, which scales inversely with environmental spectral width, and on the symmetric structure of the parameter space of the effective Hamiltonian.

To facilitate the subsequent classification, Table I lists the symbols involved in our classification of higher-order EPs together with a review of their corresponding physical meanings. In what follows, the analysis advances from the simplest to the most general case, in order of increasing parametric complexity, thereby expanding the effective dimensionality of a non-Markovian system.

First, as the simplest case, three optical cavities are coupled to three Markovian reservoirs with the parameter space satisfying the symmetry, i.e.,  $\Gamma_1 = \Gamma_2$ ,  $\lambda_1 = \lambda_2 \rightarrow \infty$  (when the environmental spectral width is board, e.g.,  $\lambda_1 = \lambda_2 = 200\text{MHz}$  in practice, the memory effects can be neglected),  $\gamma_1 = \gamma_2$ ,  $g_1 = g_2$ , and  $J = 0$ ; its effective Hamiltonian exhibits a symmetric  $3 \times 3$  structure, whose eigenspectrum only allows the emergence of EP3. Moreover, once the symmetric structure is broken, e.g.,  $\gamma_1 \neq \gamma_2$ ,  $g_1 \neq g_2$ , and  $J \neq 0$ , the eigenspectrum undergoes asymmetric splitting, giving rise to EP2 in addition to EP3.

Second, we consider the case where a symmetric system is effectively coupled to a non-Markovian environment. The cavity  $a$  is connected to two identical non-Markovian structured reservoirs, while cavities  $b_1$  and  $b_2$  are coupled to Markovian ones, i.e.,  $\Gamma_1 = \Gamma_2$ ,  $\lambda_1 = \lambda_2 = 3.77\text{MHz}$  (a narrow environmental spectral width leads to significant memory effects),  $\gamma_1 = \gamma_2$ ,  $g_1 = g_2$ , and  $J = 0$ , yields a  $4 \times 4$  effective Hamiltonian, thus EP4 emerges. Furthermore, we consider the case where an asymmetric system is coupled to two non-Markovian environments. In this case, cavity  $a$  is driven by two different non-Markovian structured reservoirs, while cavities  $b_1$  and  $b_2$  remain coupled to Markovian ones, i.e.,  $\Gamma_1 \neq \Gamma_2$ ,  $\lambda_1 \neq \lambda_2$  (each exhibits a narrow environmental spectral width, e.g.,  $\lambda_1 = 0.079\text{MHz}$  and  $\lambda_2 = 2.921\text{MHz}$ ), with all other parameters chosen appropriately. As a result, the system is governed by a  $5 \times 5$  effective Hamiltonian, which allows the emergence of EP5. The relevant details are provided in Appendix B.

Third, on the premise that cavity  $a$  is connected to two different non-Markovian structured reservoirs, we further consider the case where either  $b_1$  or  $b_2$  is coupled to a non-Markovian reservoir, i.e.,  $\Gamma_1 \neq \Gamma_2$ ,  $\lambda_1 \neq \lambda_2$  (both with narrow environmental spectral widths), and  $\Lambda_{1(2)}$  also with a narrow spectral width of the environment, while the remaining parameters are set suitably. In this case, the system interacts with three distinguishable non-Markovian environments, leading to a  $6 \times 6$  effective Hamiltonian that supports the emergence of EP6. Extending to the most general scenario, all three optical cavities couple to distinguishable non-Markovian environments, that is, cavity  $a$  is connected to two different non-Markovian structured reservoirs, while  $b_1$  and  $b_2$  each couple to a distinct non-Markovian structured reservoir, i.e.,  $\Gamma_1 \neq \Gamma_2$ ,  $\lambda_1 \neq \lambda_2$ ;  $\Upsilon_1 \neq \Upsilon_2$ ,  $\Lambda_1 \neq \Lambda_2$ ; while the other parameters taken suitably. Accordingly, the system is equivalent to being coupled to four different non-Markovian environments, resulting in a  $7 \times 7$  effective Hamiltonian and thus allowing the observation of EP7.

The above analysis confirms a common intuition: each distinguishable non-Markovian structured reservoir with a Lorentzian spectrum increases the dimension of the effective Hamiltonian by one. This conclusion is consistent with pseudomode theory, where coupling an optical mode to a non-Markovian reservoir is equivalently mapped to its coupling with an auxiliary mode that in turn interacts with a Markovian reservoir, thereby reflecting the expansion of the parameter space induced by memory effects. Physically, the memory effect rooted in non-Markovian environments scales inversely with the environmental spectral width, becoming significant for narrow widths and manifesting as an enlargement of the effective Hamiltonian, thereby giving rise to higher-order EPs. In other words, the introduction of memory effects increases the complexity of the parameter space of the system, thereby inducing the emergence of higher-order EPs.

#### IV. EXPERIMENTAL ANALYSIS

Building on our theoretical predictions, we concisely discuss the experimental feasibility and candidate superconducting circuit platforms for validating our findings. First of all, the high tunability of superconducting circuits provides solid support for the observation of higher-order EPs. Typical superconducting cavities have characteristic frequencies of order GHz, with loss rates on the order of MHz [136]. Moreover, embedding a superconducting quantum interference device (SQUID) in the cavity enables in-situ frequency tuning via the bias magnetic flux threading the SQUID loop [7]. The superconducting inter-cavity coupling strength has been experimentally verified to be tunable across a broad MHz range [137]. Additionally, the gain induced by coherent perfect absorption can be implemented by regulating the driving fields of an auxiliary superconducting qubit transversely coupled to the cavity, reaching magnitudes on the order of MHz [135]. Taken together, advances in superconducting circuits substantiate the experimental feasibility of our proposal.

Secondly, recent superconducting-circuit experiments have demonstrated the observation of EP2 and EP3 using two distinct experimental designs. The first employs a chiral quantum interconnect with a Markovian bath, where four superconducting qubits are arranged in a square and coupled pairwise, enabling the observation of EP2 [132–134]. The second is based on a non-Markovian structured bath, engineered by coupling a Josephson-junction qubit to a leaky electromagnetic resonator. This setup includes a bus resonator and tunable Xmon qubits, each individually connected to a readout resonator, which not only provides a decay channel but also coherently couples the qubit levels and thereby enhances the effective dimensionality of the system, enabling the observation of both EP2 and EP3 [138]. In principle, both schemes hold promise for the observation of higher-order EPs.

Thirdly, as an illustrative case, we analyze how EP4 can be observed in a three-mode optical system within the two experimental platforms outlined above. In the former setup, a chiral quantum interconnect with a Markovian bath effectively describes the coupling between a three-mode optical system and

a non-Markovian bath, which under the pseudomode mechanism is equivalent to a four-mode optical system coupled to a Markovian structured reservoir. With pairwise couplings replaced by all-to-all couplings, the system attains four effective degrees of freedom, making the observation of EP4 feasible. In the latter setup, multiple Xmon qubits are controllably coupled to their readout resonators, which act as non-Markovian structured reservoirs with a continuum of bosonic modes. The EPs are constructed from these qubits together with their readout resonators, where the unique non-Markovian effects enable the simultaneous emergence of higher-order EPs of different orders at the same control parameter but with different qubit numbers.

## V. CONCLUSION AND DISCUSSION

To summarize, we have studied a pseudo-Hermitian optical system [155] of three coupled cavities interacting with non-Markovian structured reservoirs. We demonstrated that memory effects rooted in non-Markovianity effectively expand the dimensionality of the effective Hamiltonian, thereby enabling the emergence of higher-order EPs. We have also observed that the pseudo-Hermitian system, with an effective gain induced by coherent perfect absorption, enables higher-order EPs to be directly identified in the output spectrum. We systematically classified higher-order EPs under different parameter-space symmetries and structured-reservoir configurations, and revealed a general rule in agreement with pseudomode theory: coupling to multiple distinguishable non-Markovian structured reservoirs with Lorentzian spectra enlarges the Hamiltonian dimension, which in turn increases the parametric complexity and yields higher-order EPs. In addition, possible experimental schemes based on a superconducting circuit were also discussed, which provide feasible routes for observing our findings.

The results of this work are nevertheless restricted to the rotating-wave approximation and to non-Markovian structured reservoirs whose spectral densities are described by a Lorentzian shape.

In the future, it is important to analyze scenarios beyond the rotating-wave approximation [102, 156–158], incorporating counter-rotating terms such as anisotropic non-rotating-wave interactions [159–162], which will broaden the applicability and generality of our theory. Another interesting direction is to realize arbitrary-order EPs within a single environment by engineering non-Markovian structured reservoirs with non-Lorentzian spectral density. Specifically, our work demonstrates a one-to-one correspondence between the number of non-Markovian structured reservoirs with Lorentzian spectral densities and the order of the resulting higher-order EPs. However, by suitably engineering a single non-Markovian reservoir with a non-Lorentzian spectral density, it may be possible to realize arbitrary-order EPs. An extreme example is that a single non-Markovian structured reservoir with an Ohmic spectral density can give rise to EPs of arbitrarily high order, up to infinity. The analysis of higher-order EPs induced by non-Markovian structured reservoirs offers new in-

sights and effective pathways for designing quantum devices with enhanced sensitivity under realistic conditions

## ACKNOWLEDGMENTS

C. S. thanks Dr. Aziza Almanaky from MIT for valuable discussions on the experimental feasibility, both in person during the RIKEN visit and subsequently by email. C. S. also thanks Dr. Hui Wang from Franco Nori's group for helpful discussions. This work was supported by the Science and Technology Development Plan Project of Jilin Province (Grant No. 20250102007JC), and the National Natural Science Foundation of China under Grant No. 12274064. C. S. acknowledges financial support from the China Scholarship Council, the Japanese Government (Monbukagakusho-MEXT) Scholarship (Grant No. 211501), the RIKEN Junior Research Associate Program, and the Hakubi Projects of RIKEN.

## DATA AVAILABILITY

The data that support the findings of this study are available on request from the corresponding authors H. Z. Shen and Cheng Shang.

## Appendix A: Pseudomode analysis

Within the pseudomode framework, a structured bath is replaced by a set of locally damped auxiliary modes that reproduce its spectral density [163]. As an example, for a cavity mode, this Markovian embedding realizes a controllable Lorentzian bath spectral density in a non-Markovian environment [164–171]. We introduce a system composed of a cavity mode (eigenfrequency  $\omega_n$ ) coupled to a pseudomode (eigenfrequency  $\omega_x$ ). The Hamiltonian for this system is

$$H_S = \omega_n n^\dagger n + \omega_x x^\dagger x + g_{nx} (n x^\dagger + n^\dagger x), \quad (\text{A1})$$

where the first and second terms on the right-hand side are the free Hamiltonians of the cavity and the pseudomode, respectively. Their annihilation operators,  $n$ ,  $x$ , satisfy the bosonic commutation relations  $[n, n^\dagger] = [x, x^\dagger] = 1$ . The last term in Eq. (A1) corresponds to the tunneling coupling between the cavity mode and the pseudomode with the coupling strength  $g_{nx}$ . The corresponding total Hamiltonian including the Markovian environment reads

$$H_T = H_S + H_R + H_I, \quad (\text{A2})$$

where  $H_I = i \sum_k V_k (q_k^\dagger x - x^\dagger q_k)$  denotes the interaction Hamiltonian between the pseudomode and the Markovian environment, with  $V_k = \sqrt{\gamma/2\pi}$  and  $\gamma$  representing the coupling strength and decay rate, respectively. The free Hamiltonian of the environment is given by  $H_R = \sum_k \omega_k q_k^\dagger q_k$ , which

satisfies the commutation relation  $[q_k, q_{k'}^\dagger] = \delta_{kk'}$ . According to Eq. (A2), the Heisenberg-Langevin equations under the Markovian approximation take the form [69, 151]

$$\frac{d}{dt}n = -i\omega_n n - ig_{nx}x, \quad (\text{A3})$$

$$\frac{d}{dt}x = -ig_{nx}n - \frac{\gamma}{2}x - \sqrt{\gamma}q_{\text{in}}(t). \quad (\text{A4})$$

Solving Eq. (A4) for  $x(t)$  gives  $x(t) = x(0)e^{-\frac{\gamma}{2}t} - ig_{nx}\int_0^t n(\tau)e^{-\frac{\gamma}{2}(t-\tau)}d\tau - \sqrt{\gamma}\int_0^t q_{\text{in}}(\tau)e^{-\frac{\gamma}{2}(t-\tau)}d\tau$  with  $q_{\text{in}}(t) = \sum_k e^{-i\omega_k t}q_k/\sqrt{2\pi}$ . Substituting  $x(t)$  into Eq. (A3), we obtain

$$\frac{d}{dt}n = -i\omega_n n - \int_0^t \beta(t-\tau)n(\tau)d\tau - R(t), \quad (\text{A5})$$

where  $R(t) = ig_{nx}x(0)e^{-\frac{\gamma}{2}t} - ig_{nx}\sqrt{\gamma}\int_0^t q_{\text{in}}(\tau)e^{-\frac{\gamma}{2}(t-\tau)}d\tau$  is the operator for the non-Markovian composite environment, which comprises the pseudomode and its Markovian environment, and  $\beta(t) = g_{nx}^2 e^{-\frac{\gamma}{2}t}$  is the corresponding correlation function. The Lorentzian spectrum density  $S(\omega)$  corresponding to the correlation function  $\beta(t) = g_{nx}^2 e^{-\frac{\gamma}{2}t} \equiv \int S(\omega)e^{-i\omega t}d\omega$  in Eq. (A5) is equal to Eq. (11), where

$$\lambda_1 = \frac{\gamma_1}{2}, \lambda_2 = \frac{\gamma_2}{2}, \Gamma_1 = \frac{4g_{nx}^2}{\gamma_1}, \Gamma_2 = \frac{4g_{nx}^2}{\gamma_2}, \quad (\text{A6})$$

which leads to

$$\begin{aligned} \beta_1(t-\tau) &= \frac{1}{2}\Gamma_1\lambda_1 e^{-\lambda_1(t-\tau)}, \\ \beta_2(t-\tau) &= \frac{1}{2}\Gamma_2\lambda_2 e^{-\lambda_2(t-\tau)}, \end{aligned} \quad (\text{A7})$$

which is consistent with  $f_1(t)$  and  $f_2(t)$  below Eq. (10). Defining the expectation values of the operators as  $n := \langle n \rangle$ ,  $x := \langle x \rangle$ ,  $q_k := \langle q_k \rangle$ ,  $q_{\text{in}} := \langle q_{\text{in}} \rangle$ ,  $R(t) := \langle R(t) \rangle$ ,  $a_{\text{in}} := \langle a_{\text{in}} \rangle$ ,  $K(t) := \langle K(t) \rangle$ ,  $c := \langle c \rangle$ , and considering

$$K(t) = -R(t), \quad (\text{A8})$$

we obtain

$$q_{\text{in}}(t) = \frac{\gamma}{2}c(t) + c'(t), \quad (\text{A9})$$

$$x = \frac{i}{g_{nx}} \int_{-\infty}^{+\infty} h^*(-\tau)a_{\text{in}}(\tau)d\tau, \quad (\text{A10})$$

with

$$c(t) = \frac{g_{nx}xe^{-\frac{\gamma}{2}t} - iK(t)}{g_{nx}\sqrt{\gamma}}, \quad (\text{A11})$$

$$K(t) = \int_{-\infty}^{+\infty} h^*(t-\tau)a_{\text{in}}(\tau)d\tau. \quad (\text{A12})$$

The value of  $x = \text{Tr}[x(0)\rho_x(0)]$  is determined by the initial state  $\rho_x(0)$  of the pseudomode. If  $x$  takes

$$x = i \frac{\sqrt{\Gamma}\lambda}{g_{nx}} \int_0^{+\infty} e^{-\lambda\tau} a_{\text{in}}(\tau)d\tau, \quad (\text{A13})$$

then by comparing Eq. (A10) and Eq. (A13), we obtain

$$\begin{aligned} h_1(t) &= \sqrt{\Gamma_1}\lambda_1 e^{\lambda_1 t}\vartheta(-t), \\ h_2(t) &= \sqrt{\Gamma_2}\lambda_2 e^{\lambda_2 t}\vartheta(-t), \end{aligned} \quad (\text{A14})$$

which correspond to  $\kappa_1(t)$  and  $\kappa_2(t)$  in the main text, respectively. Here,  $n$  represent  $a$ ,  $b_1$ , and  $b_2$ . This relation is valid according to Eq. (A14). Therefore, when Eqs. (A7), (A9), (A10), and (A13) are satisfied simultaneously, we demonstrate that the equations derived from the Markovian pseudomode method are completely consistent with Eq. (6) in the non-Markovian regime.

## Appendix B: General case of two different non-Markovian structured reservoirs

For the general case, we consider  $\lambda_1 \neq \lambda_2$  and  $\Gamma_1 \neq \Gamma_2$ , which leads to  $K_1(t) \neq K_2(t)$ , where the integral equation of operator  $a$  is shown in Eq. (6). When the spectral widths of the non-Markovian environments at the two ports are unequal, the effective non-Hermitian Hamiltonian can be formulated as a fifth-order matrix

$$H_{N_5} = \begin{pmatrix} \Delta_a & g_1 & g_2 & -ih_1 & -ih_2 \\ g_1 & \Delta_{b_1} - i\gamma_1 & J & 0 & 0 \\ g_2 & J & \Delta_{b_2} - i\gamma_2 & 0 & 0 \\ ih_1 & 0 & 0 & i\lambda_1 & 0 \\ ih_2 & 0 & 0 & 0 & i\lambda_2 \end{pmatrix}, \quad (\text{B1})$$

where  $h_1 = \sqrt{\lambda_1\Gamma_1/2}$  and  $h_2 = \sqrt{\lambda_2\Gamma_2/2}$ . The characteristic equation for the eigenvalue  $x$  can be written as

$$a'x^5 + b'x^4 + c'x^3 + d'x^2 + e'x + f' = 0. \quad (\text{B2})$$

For the quintic equation, we define the discriminants  $\Delta_{b_1} := B'^2 - 4A'C'$  and  $\Delta_{b_2} := P'^2 - 4L'^5$ . Then, Eq. (B2) has a quintuple real root if and only if  $B'^2 - 4A'C' = 0$  and  $P'^2 - 4L'^5 = 0$  hold simultaneously. Here,  $A'$ ,  $B'$  and  $C'$  are given by  $A' = F'^2 - 12E'^2L'$ ,  $B' = 6F'^3 - 64E'^2F'L' - 72E'^3M'$ ,  $C' = 3F'^4 - 24E'^2F'^2L' - 48E'^3F'M' - 80E'^4L'^2$ , where  $E' = 2G'^2L'^2 - 2G'^2N' + 3G'H'M' - 4H'^2L' - G'JL'$ ,  $F' = G'^2P' + 3G'JM' - 4H'JL'$ ,  $G' = 4L'^3 - 9M'^2 + 8L'N'$ ,  $H' = 10L'^2M' - 6M'N' + L'P'$ , and  $J = 4L'^4 - 4L'^2N' + 3M'P'$ . Additionally,  $\{A', B', C'\}$  are also related to  $\{L', M', N', P'\}$  with

$$L' = 2b'^2 - 5a'c',$$

$$M' = 4b'^3 - 15a'b'c' + 25a'^2d', \quad (\text{B3})$$

$$N' = 7b'^4 + 25a'^2c'^2 - 35a'b'^2c' + 50a'^2b'd' - 125a'^3e',$$

$$P' = 4b'^5 - 25a'b'^3c' + 125a'^2b'^2d' - 625a'^3b'e' + 3125a'^4f'.$$

When  $L' = M' = N' = P' = 0$ , Eq. (B2) has a quintuple real root, where  $x_1 = x_2 = x_3 = x_4 = x_5$ , and

$$x_5 = -\frac{b'}{5a'} = -\frac{c'}{2b'} = -\frac{d'}{c'} = -\frac{2e'}{d'} = -\frac{5f'}{e'}. \quad (\text{B4})$$

Following this, we will explore the determination of the parametric conditions necessary to guarantee the pseudo-Hermiticity of the effective Hamiltonian  $H_{N_5}$  in Eq. (B1). By following the procedure described in Ref. [46],  $H_{N_5}$  acquires pseudo-Hermitian properties provided that its eigenvalues satisfy a requirement, that is, all five eigenvalues must be real. To verify this condition, we solve the equation  $\text{Det}(H_{N_5\text{eff}} - \Omega I) = 0$ , that is

$$\left| \begin{array}{ccccc} \Delta_a - \Omega & g_1 & g_2 & -ih_1 & -ih_2 \\ g_1 & M_1 & J & 0 & 0 \\ g_2 & J & M_2 & 0 & 0 \\ ih_1 & 0 & 0 & i\lambda_1 - \Omega & 0 \\ ih_2 & 0 & 0 & 0 & i\lambda_2 - \Omega \end{array} \right| = 0, \quad (\text{B5})$$

$$\begin{aligned} \lambda_1 &= \gamma_1 + \gamma_2 - \lambda_2, \quad \Delta_{b_1} = \frac{-\Delta_{b_2}\gamma_2}{\gamma_1}, \quad \zeta = -\gamma_2 + \frac{\gamma_1^2(\gamma_1 + \gamma_2 - \lambda_2)^2}{J^2\gamma_1 + (\Delta_{b_2}^2 + \gamma_1^2)\gamma_2}, \\ \Delta_a &= \frac{-2g_1^2\Delta_{b_2}\gamma_1^2\gamma_2 + 2g_1g_2J\gamma_1^2(\gamma_1 + \gamma_2) + \Delta_{b_2}(2g_2^2\gamma_1^2\gamma_2 + J^2\gamma_1(\gamma_1^2 - \gamma_2^2) + (\omega_2^2 + \gamma_1^2)(\gamma_1 - \gamma_2)\gamma_2(\gamma_1 + \gamma_2))}{\gamma_1(\gamma_1 + \gamma_2)(J^2\gamma_1 + \Delta_{b_2}^2\gamma_2 + \gamma_1(\gamma_1 - \lambda_2)(\gamma_2 - \lambda_2))}, \\ \Gamma_1 &= \frac{2(g_1^2\gamma_1^2 + g_2^2\gamma_1\gamma_2 + J^2\gamma_1(\gamma_1 + \gamma_2) + (\Delta_{b_2}^2 + \gamma_1^2)\gamma_2(\gamma_1 + \gamma_2)) - 2\gamma_1(\gamma_1 + \gamma_2)^2\lambda_2 + \gamma_1(2(\gamma_1 + \gamma_2) - \Gamma_2)\lambda_2^2}{\gamma_1(\gamma_1 + \gamma_2 - \lambda_2)^2}, \\ \Gamma_2 &= \frac{2}{\lambda_1 - \lambda_2}(-J^2 + \Delta_{b_2}\Delta_{b_1} - \gamma_1\gamma_2 - \frac{g_1^2\gamma_1(J^2\gamma_1 + \gamma_2(\Delta_{b_2}^2 - (\gamma_2 - \lambda_2)(2\gamma_1 + \gamma_2 - \lambda_2)))}{(\gamma_1 + \gamma_2)(J^2\gamma_1 + (\Delta_{b_2}^2 + \gamma_1^2)\gamma_2)} + \frac{g_2^2\zeta}{\gamma_1 + \gamma_2} - \epsilon + \lambda_1\lambda_2), \\ \epsilon &= \frac{\Delta_{b_2}(\gamma_1 - \gamma_2)(-2g_1^2\Delta_{b_2}\gamma_1^2\gamma_2 + 2g_1g_2J\gamma_1^2(\gamma_1 + \gamma_2) + \Delta_{b_2}(2g_2^2\gamma_1^2\gamma_2 + (\gamma_1^2 - \gamma_2^2)(J^2\gamma_1 + (\Delta_{b_2}^2 + \gamma_1^2)\gamma_2)))(\lambda_1)^2}{\gamma_1(\gamma_1 + \gamma_2)(J^2\gamma_1 + (\Delta_{b_2}^2 + \gamma_1^2)\gamma_2)(J^2\gamma_1 + \Delta_{b_2}^2\gamma_2 + \gamma_1(\gamma_1 - \lambda_2)(\gamma_2 - \lambda_2))}. \end{aligned} \quad (\text{B7})$$

In Fig. 5, we consider the most general case where the dissipations of cavity  $b_1$  and cavity  $b_2$  are different, which are denoted as  $\gamma_1 \neq \gamma_2$ , for example with  $\gamma_1 = 2\gamma_2 = 2$  MHz. Figure 5(a) and 5(b) respectively show the real and imaginary parts of the eigenvalues as functions of  $g_1$  in the non-Markovian case with the critical coupling strength  $g_{\text{EP5}} = 1.5$  MHz at EP. When  $g_1 < g_{\text{EP5}}$ , the five eigenvalues manifest as one real and two pairs of complex conjugates. At  $g_1 = g_{\text{EP5}}$  (i.e., at EP5), the five eigenvalues coalesce into a real number. With the parameter  $g_2$  fixed at 0.589 MHz, the eigenvalues evolve as follows: when  $g_1 > g_{\text{EP5}}$ , they appear as three real values and one pair of complex conjugates. Figure 5(c) and 5(d) plot the real and imaginary parts of the eigenvalues as functions of  $g_1$  during the conversion from non-Markovian to Markovian regimes. Comparing them with Fig. 5(e) and 5(f), the difference lies in the presence of two lines with real parts equal to zero and imaginary parts that correspond to the spectral widths of the non-Markovian environments ( $\Omega_4$  and  $\Omega_5$ ). In this case, the critical coupling strength is  $g_{\text{EP3}}(g_{\text{EP5}})/2\pi = 2.258$  MHz. When  $g_1 < g_{\text{EP3}}$ , three eigenvalues are observed as one real and one pair of complex

where  $M_1 = (\Delta_{b_1} - i\gamma_1) - \Omega$  and  $M_2 = (\Delta_{b_2} - i\gamma_2) - \Omega$ .

We can derive the five eigenvalues based on the energy-spectrum properties described in the pseudo-Hermitian Hamiltonian formalism [46] by considering the complex conjugate of Eq. (B5), i.e.,  $\text{Det}(H_{N_5\text{eff}}^* - \Omega I) = 0$ , which gives

$$\left| \begin{array}{ccccc} \Delta_a - \Omega & g_1 & g_2 & ih_1 & ih_2 \\ g_1 & M_1^* & J & 0 & 0 \\ g_2 & J & M_2^* & 0 & 0 \\ -ih_1 & 0 & 0 & -i\lambda_1 - \Omega & 0 \\ -ih_2 & 0 & 0 & 0 & -i\lambda_2 - \Omega \end{array} \right| = 0, \quad (\text{B6})$$

where  $M_1^* = (\Delta_{b_1} + i\gamma_1) - \Omega$  and  $M_2^* = (\Delta_{b_2} + i\gamma_2) - \Omega$ . Comparing Eqs. (B5) and (B6) gives the constraint

conjugates. At  $g_1 = g_{\text{EP3}}$ , i.e., at EP3, the three eigenvalues coalesce into a real number. When  $g_1 > g_{\text{EP3}}$ , the eigenvalues appear as another real and one pair of complex conjugates. The remaining parameters are set to  $g_2/2\pi = 1.125$  MHz,  $\Gamma_1/2\pi = 4$  MHz, and  $\Gamma_2/2\pi = 2$  MHz. We can observe the conversion from a fifth-order exceptional point in a non-Markovian pseudo-Hermitian system to a third-order exceptional point in a Markovian system.

### Appendix C: Derivation and discussion of Eq. (13)

Using the modified Laplace transformation [149, 153, 154]

$$\eta(\omega) = \int_0^\infty e^{i\omega t} \eta(t) dt, \quad (\text{C1})$$

$\exp(i\omega t) \rightarrow \exp(i\omega t - \epsilon t)$  with  $\epsilon \rightarrow 0^+$  makes  $\eta(\omega)$  converge to a finite value. With the definitions  $\sqrt{2\pi}a(t) = \int_0^{+\infty} a(\omega)e^{-i\omega t} d\omega$  and  $\sqrt{2\pi}b_j(t) = \int_0^{+\infty} b_j(\omega)e^{-i\omega t} d\omega$ , the Heisenberg-Langevin equations from Eq. (12) can be transformed into Eq. (13).

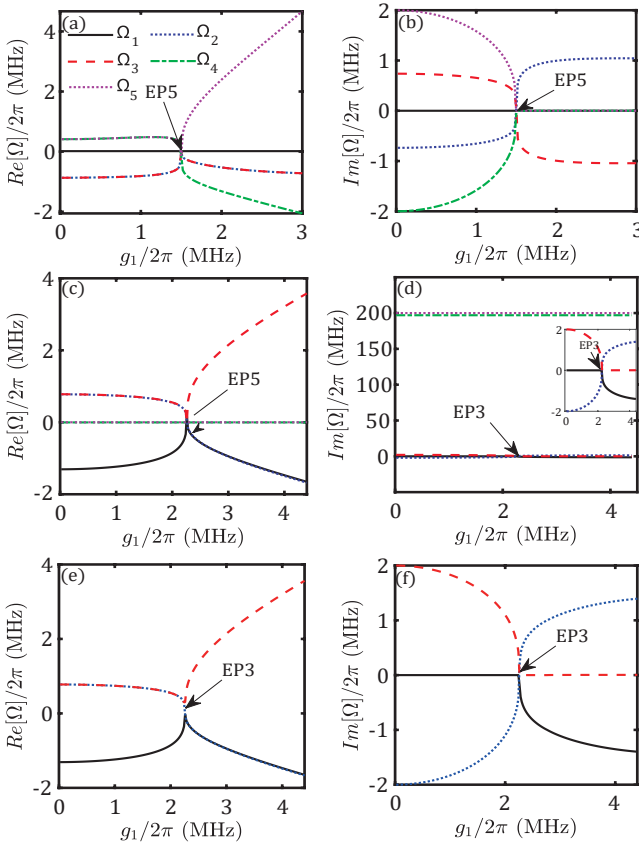


FIG. 5. Based on Eq. (B1), the conversion of eigenvalues from the non-Markovian to the Markovian regime at the EPs is analyzed as a function of the coupling strength  $g_1$ . (a) and (b) respectively plot the real and imaginary parts of the eigenvalues of the effective Hamiltonian  $H_{N5}$  in the non-Markovian case with  $\lambda_1/2\pi = 0.079$  MHz and  $\lambda_2/2\pi = 2.921$  MHz. (c) and (d) display the real and imaginary parts of the eigenvalues during the conversion to the Markovian regime, corresponding to  $\lambda_1/2\pi = 200$  MHz and  $\lambda_2/2\pi = 220$  MHz. (e) and (f) present the real and imaginary parts under the Markovian approximation, with parameters  $\gamma_1/2\pi = 2$  MHz and  $\gamma_2/2\pi = 1$  MHz.

Our goal is to evaluate the impact of the non-homogeneous terms,  $a_{in}^{(1)}(i\lambda_1)$  and  $a_{in}^{(2)}(i\lambda_2)$ , in Eq. (13), where  $\lambda_1$  and  $\lambda_2$  denote the spectral widths of the non-Markovian input environments at ports 1 and 2, respectively. Taking  $a_{in}^{(1)}(t)$  as an illustrative example, we set  $\phi(\lambda_1, \omega) = a_{in}^{(1)}(i\lambda_1)/a_{in}^{(1)}(\omega)$ . The input field takes two forms: a damped-oscillation form expressed as  $a_{in}^{(1)}(t) = xe^{-zt} \sin(yt^2)$  with  $z > 0$  and  $y > 0$ , and a Gaussian-profile form given by  $a_{in}^{(1)}(t) = xe^{-zt^2} \cos(yt)$ . These two forms give concrete expressions for  $\phi(\lambda_1, \omega)$ . For the damped-oscillation form:  $\phi(\lambda_1, \omega) = \{\cos[\frac{(\lambda+z)^2}{4y}][1 - 2fc(\frac{\lambda+z}{\sqrt{2\pi y}})] + [1 - 2fs(\frac{\lambda+z}{\sqrt{2\pi y}})]\sin[\frac{(\lambda+z)^2}{4y}]\}/\{\cos[\frac{(z-i\omega)^2}{4y}][1 - 2fc(\frac{z-i\omega}{\sqrt{2\pi y}})] + [1 - 2fs(\frac{z-i\omega}{\sqrt{2\pi y}})]\sin[\frac{(z-i\omega)^2}{4y}]\}$ . On the other hand, for the Gaussian - profile form:  $\phi(\lambda_1, \omega) = e^{\frac{\lambda^2 + \omega^2 + 2y(\omega - i\lambda)}{4z}} \{i +$

$e^{\frac{iy\lambda}{z}} [i + \text{erfi}(\frac{y-i\lambda}{2\sqrt{z}}) - \text{erfi}(\frac{y+i\lambda}{2\sqrt{z}})]\} / \{i + e^{\frac{y\omega}{z}} [i + \text{erfi}(\frac{y-\omega}{2\sqrt{z}}) - \text{erfi}(\frac{y+\omega}{2\sqrt{z}})\}$ , where  $fc(\psi) = \int_0^\psi \cos(\pi t^2/2) dt$ ,  $fs(\psi) = \int_0^\psi \sin(\pi t^2/2) dt$ , and  $\text{erfi}(\psi) = -ierf(i\psi)$ . These non-homogeneous terms are determined by the forms of the input field  $a_{in}^{(1)}(t)$ . In the Markovian approximation, as  $\lambda_1 \rightarrow \infty$ ,  $\phi(\lambda_1, \omega)$  approaches zero.

We find that the non-homogeneous terms are incapable of uncovering the characteristics of the systems being probed. For the damped-oscillation form, when  $\lambda = \omega_\nu$ , which falls in the non-Markovian regimes, we can estimate  $|\phi(\lambda_1, \omega)| \approx 6 \times 10^{-6}$ , and when  $\lambda = 9\omega_\nu$ , where weak non-Markovian effects are present,  $|\phi(\lambda_1, \omega)| \approx 8 \times 10^{-9}$ , where  $z = 0.0001\omega_\nu$ ,  $y = 0.00015\omega_\nu$ , and  $\omega = \omega_\nu$ . For the Gaussian-profile form, by choosing the same parameters as in the damped-oscillation case, we find that  $|\phi(\lambda_1, \omega)| \approx 0$  when  $\lambda = \omega_\nu$  and  $\lambda = 9\omega_\nu$ . The non-homogeneous term  $a_{in}^{(1)}(i\lambda_1)$  is significantly smaller than  $a_{in}^{(1)}(\omega)$  and can be neglected for these parameter values. Similar discussions and conclusions can be drawn for the term  $a_{in}^{(2)}(i\lambda_2)$ . Consequently, we can safely neglect the influence of the inhomogenous terms on the system dynamics.

#### Appendix D: Analysis of parameter-space asymmetry

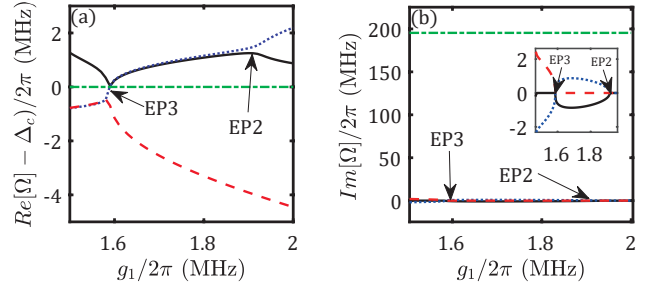


FIG. 6. The evolution of the eigenvalues for the effective Hamiltonian associated with Eq. (1) as the coupling strength  $g$  varies, at environmental spectral width  $\lambda_1/2\pi = \lambda_2/2\pi = 200$  MHz. Herein, (a) and (b) present the real and imaginary parts of these eigenvalues. We set the asymmetry parameters to  $\gamma_2 = 2\gamma_1$  and  $g_2 = 2g_1$ . The remaining parameters are set to  $\Gamma_1/2\pi = \Gamma_2/2\pi = 4.5$  MHz.

Figure 6(a) and 6(b) show the changes in the real and imaginary parts of the eigenvalues during the non-Markovian to Markovian regimes under the asymmetric case with  $\gamma_2 = 2\gamma_1$  and  $g_2 = 2g_1$ . The comparison with Markovian case highlights the addition of green dashed-dotted lines in both the real and imaginary parts, serving to identify the zero eigenvalue and the spectral width feature of the non-Markovian environments, respectively. Notably, in the asymmetric-parameter regime, an EP2 emerges that is absent in the symmetric case. This arises from eigenvalue splitting induced by the breaking of parameter-space symmetry.

## Appendix E: Details of the classification of higher-order EPs

Regarding the discussion and analysis of EP5, Appendix B has already been discussed and will not be elaborated further here. In the following discussion, we consider that the environments of the two ports of the cavity  $a$  are in non-Markovian regimes, and also the environments of the cavities  $b_1$  and  $b_2$ , where the environments are composed of a series of bosonic modes. The cavity is coupled to the  $k$ th mode of the non-Markovian environments via the annihilation operators  $e_k, f_k$ , and their respective creation operators  $e_k^\dagger, f_k^\dagger$ , with the mode eigenfrequencies being  $\alpha_k$  and  $\beta_k$ , respectively. The total non-Markovian Hamiltonian in Eq. (1) becomes

$$\begin{aligned}
H'_T = & \Delta_a a^\dagger a + \sum_{j=1,2} \left[ \Delta_{b_j} b_j^\dagger b_j + g_j (a^\dagger b_j + a b_j^\dagger) \right] \\
& + J(b_1^\dagger b_2 + b_1 b_2^\dagger) + \sum_k \Omega_k c_k^\dagger c_k + \sum_k \varpi_s d_s^\dagger d_s \\
& + \sum_k \alpha_k e_k^\dagger e_k + \sum_k \beta_k f_k^\dagger f_k + i \sum_k (C_k a c_k^\dagger - C_k^* a^\dagger c_k) \\
& + i \sum_k (D_s a d_s^\dagger - D_s^* a^\dagger d_s) + i \sum_k (A_k b_1 e_k^\dagger - A_k^* b_1^\dagger e_k) \\
& + i \sum_k (B_k b_2 f_k^\dagger - B_k^* b_2^\dagger f_k), \tag{E1}
\end{aligned}$$

where  $C_k, D_s, A_k$  and  $B_k$  denote the interaction strengths for the cavity  $a$  at ports 1 and 2, the cavity  $b_1$  and the cavity  $b_2$  with their respective non-Markovian environments, which have intrinsic frequencies  $\Omega_k, \varpi_s, \alpha_k$ , and  $\beta_k$ , respectively. With Eq. (E1), the Heisenberg equation reads

$$\begin{aligned}
\frac{d}{dt} a(t) = & -i\Delta_a a(t) - ig_1 b_1(t) - ig_2 b_2(t) - \sum_k C_k^* c_k(t) \\
& - \sum_k D_s^* d_s(t), \\
\frac{d}{dt} b_1(t) = & -i\Delta_{b_1} b_1(t) - ig_1 a(t) - iJ b_2(t) - \sum_k A_k^* e_k(t), \\
\frac{d}{dt} b_2(t) = & -i\Delta_{b_2} b_2(t) - ig_2 a(t) - iJ b_1(t) - \sum_k B_k^* f_k(t), \\
\frac{d}{dt} c_k(t) = & -i\Omega_k c_k(t) + C_k a(t), \tag{E2} \\
\frac{d}{dt} d_s(t) = & -i\varpi_s d_s(t) + D_s a(t), \\
\frac{d}{dt} e_k(t) = & -i\alpha_k e_k(t) + A_k b_1(t), \\
\frac{d}{dt} f_k(t) = & -i\beta_k f_k(t) + B_k b_2(t).
\end{aligned}$$

By solving Eq. (E2), we obtain the environmental operators as follows

$$\begin{aligned}
c_k(t) = & c_k(0) e^{-i\Omega_k t} + C_k \int_0^t a(\tau) e^{-i\Omega_k(t-\tau)} d\tau, \\
d_s(t) = & d_s(0) e^{-i\varpi_s t} + D_s \int_0^t a(\tau) e^{-i\varpi_s(t-\tau)} d\tau, \\
e_k(t) = & e_k(0) e^{-i\alpha_k t} + A_k \int_0^t b_1(\tau) e^{-i\alpha_k(t-\tau)} d\tau, \\
f_k(t) = & f_k(0) e^{-i\beta_k t} + B_k \int_0^t b_2(\tau) e^{-i\beta_k(t-\tau)} d\tau, \tag{E3}
\end{aligned}$$

where the first term reflects the free evolution of the non-Markovian environmental fields, while the second term captures the non-Markovian feedback effects from the environments onto the cavities. By substituting Eq. (E3) into Eq. (E2), we derive the non-Markovian Heisenberg-Langevin equation for the cavity operators

$$\begin{aligned}
\frac{d}{dt} a(t) = & -i\Delta_a a(t) - ig_1 b_1(t) - ig_2 b_2(t) + K_1(t) + K_2(t) \\
& - \int_0^t a(\tau) f_1(t-\tau) d\tau - \int_0^t a(\tau) f_2(t-\tau) d\tau, \\
\frac{d}{dt} b_1(t) = & -i\Delta_{b_1} b_1(t) - ig_1 a(t) - iJ b_2(t) + K_3(t) \\
& - \int_0^t b_1(\tau) f_3(t-\tau) d\tau, \tag{E4} \\
\frac{d}{dt} b_2(t) = & -i\Delta_{b_2} b_2(t) - ig_2 a(t) - iJ b_1(t) + K_4(t) \\
& - \int_0^t b_2(\tau) f_4(t-\tau) d\tau,
\end{aligned}$$

where

$$\begin{aligned}
K_3(t) = & - \sum_k A_k^* e_k(0) e^{-i\alpha_k t} = \int_{-\infty}^{\infty} \kappa_3^*(t-\tau) b_1^{(\text{in})}(\tau) d\tau, \\
K_4(t) = & - \sum_k B_k^* f_k(0) e^{-i\beta_k t} = \int_{-\infty}^{\infty} \kappa_4^*(t-\tau) b_2^{(\text{in})}(\tau) d\tau, \\
b_1^{(\text{in})}(t) = & -\frac{1}{\sqrt{2\pi}} \sum_k e_k(0) e^{-i\alpha_k t}, \\
b_2^{(\text{in})}(t) = & -\frac{1}{\sqrt{2\pi}} \sum_k f_k(0) e^{-i\beta_k t}, \\
\kappa_3(t-\tau) = & \frac{1}{\sqrt{2\pi}} \int e^{i\omega(t-\tau)} A(\omega) d\omega, \\
\kappa_4(t-\tau) = & \frac{1}{\sqrt{2\pi}} \int e^{i\omega(t-\tau)} B(\omega) d\omega, \tag{E5} \\
f_3(t) = & \int S_3(\omega) e^{-i\omega t} d\omega, \quad f_4(t) = \int S_4(\omega) e^{-i\omega t} d\omega, \\
S_3(\omega) = & \sum_k |A_k|^2 \delta(\omega - \alpha_k),
\end{aligned}$$

and  $S_4(\omega) = \sum_k |B_k|^2 \delta(\omega - \beta_k)$ . Eq. (E4) can be written as a matrix form with  $\mathbf{N} = (a, b_1, b_2, Z_1, Z_2, Z_3, Z_4)^T$

$$\dot{\mathbf{N}} = -iH_{N_7}\mathbf{N}, \tag{E6}$$

where we have used the non-Markovian input-output relations in Eq. (10), defined  $b_1^{(\text{out})}(t) + b_1^{(\text{in})}(t) = \int_0^t \kappa_3(\tau-t)b_1(\tau)d\tau$ ,  $b_2^{(\text{out})}(t) + b_2^{(\text{in})}(t) = \int_0^t \kappa_4(\tau-t)b_2(\tau)d\tau$ , and imposed CPA. In Eq. (E6), the effective Hamiltonian  $H_{N_7}$  is written as

$$\begin{pmatrix} \Delta_a & g_1 & g_2 & -i\mu_1 & -i\mu_2 & 0 & 0 \\ g_1 & \Delta_{b_1} - i\gamma_1 & J & 0 & 0 & i\mu_3 & 0 \\ g_2 & J & \Delta_{b_2} - i\gamma_2 & 0 & 0 & 0 & i\mu_4 \\ i\mu_1 & 0 & 0 & i\lambda_1 & 0 & 0 & 0 \\ i\mu_2 & 0 & 0 & 0 & i\lambda_2 & 0 & 0 \\ 0 & i\mu_3 & 0 & 0 & 0 & i\lambda_3 & 0 \\ 0 & 0 & i\mu_4 & 0 & 0 & 0 & i\lambda_4 \end{pmatrix}, \quad (\text{E7})$$

where  $\mu_n := \sqrt{\lambda_n \Gamma_n / 2}$  with  $n = 1, 2, 3, 4$ . When the two non-Markovian environments coupled to cavity  $a$  are identi-

cal, the Hamiltonian  $H_{N_6}$  given by the effective Hamiltonian  $H_{N_7}$  in Eq. (E7) reduces to

$$\begin{pmatrix} \Delta_a & g_1 & g_2 & -2i\mu_1 & 0 & 0 \\ g_1 & \Delta_{b_1} - i\gamma_1 & J & 0 & i\mu_3 & 0 \\ g_2 & J & \Delta_{b_2} - i\gamma_2 & 0 & 0 & i\mu_4 \\ i\mu_1 & 0 & 0 & i\lambda_1 & 0 & 0 \\ 0 & i\mu_3 & 0 & 0 & i\lambda_3 & 0 \\ 0 & 0 & i\mu_4 & 0 & 0 & i\lambda_4 \end{pmatrix}. \quad (\text{E8})$$

Building on the Hamiltonians in Eqs. (E7) and (E8), one can analyze EP6 and EP7 in non-Markovian dynamics. The analysis proceeds in parallel with the method used in previous discussions. For brevity, we will not go into detailed discussions.

---

[1] Z. L. Xiang, S. Ashhab, J. Q. You, and F. Nori, Hybrid quantum circuits: Superconducting circuits interacting with other quantum systems, *Rev. Mod. Phys.* **85**, 623 (2013).

[2] F. Quijandría, U. Naether, Ş. K. Özdemir, F. Nori, and D. Zueco,  $\mathcal{PT}$ -symmetric circuit QED, *Phys. Rev. A* **97**, 053846 (2018).

[3] S. Dogra, A. A. Melnikov, and G. S. Paraoanu, Quantum simulation of parity-time symmetry breaking with a superconducting quantum processor, *Commun. Phys.* **4**, 26 (2021).

[4] M. Naghiloo, M. Abbasi, Y. N. Joglekar, and K. W. Murch, Quantum state tomography across the exceptional point in a single dissipative qubit, *Nat. Phys.* **15**, 1232 (2019).

[5] W. Chen, M. Abbasi, Y. N. Joglekar, and K. W. Murch, Quantum Jumps in the Non-Hermitian Dynamics of a Superconducting Qubit, *Phys. Rev. Lett.* **127**, 140504 (2021).

[6] W. Chen, M. Abbasi, B. Ha, S. Erdamar, Y. N. Joglekar, and K. W. Murch, Decoherence-Induced Exceptional Points in a Dissipative Superconducting Qubit, *Phys. Rev. Lett.* **128**, 110402 (2022).

[7] M. Partanen, J. Goetz, K. Y. Tan, K. Kohvakka, V. Sevruik, R. E. Lake, R. Kokkoniemi, J. Ikonen, D. Hazra, A. Mäkinen, E. Hyypä, L. Grönberg, V. Vesterinen, M. Silveri, and M. Möttönen, Exceptional points in tunable superconducting resonators, *Phys. Rev. B* **100**, 134505 (2019).

[8] P. R. Han, F. Wu, X. J. Huang, H. Z. Wu, C. L. Zou, W. Yi, M. Zhang, H. Li, K. Xu, D. Zheng, H. Fan, J. Wen, Z. B. Yang, and S. B. Zheng, Exceptional Entanglement Phenomena: Non-Hermiticity Meeting Nonclassicality, *Phys. Rev. Lett.* **131**, 260201 (2023).

[9] P. R. Han, W. Ning, X. J. Huang, R. H. Zheng, S. B. Yang, F. Wu, Z. B. Yang, Q. P. Su, C. P. Yang, and S. B. Zheng, Measuring topological invariants for higher-order exceptional points in quantum three-mode systems, *Nat. Commun.* **15**, 10293 (2024).

[10] G. Q. Zhang, W. Feng, Y. Wang, and C. P. Yang, Higher-order exceptional surface in a pseudo-Hermitian superconducting circuit, *arXiv:2403.06062*.

[11] L. Feng, R. El-Ganainy, and L. Ge, Non-Hermitian photonics based on parity-time symmetry, *Nat. Photonics* **11**, 752 (2017).

[12] S. Khandelwal, N. Brunner, and G. Haack, Signatures of Liouvillian Exceptional Points in a Quantum Thermal Machine, *PRX Quantum* **2**, 040346 (2021).

[13] R. El-Ganainy, K. G. Makris, M. Khajavikhan, Z. H. Musslimani, S. Rotter, and D. N. Christodoulides, Non-Hermitian physics and  $\mathcal{PT}$  symmetry, *Nat. Phys.* **14**, 11 (2018).

[14] Ş. K. Özdemir, S. Rotter, F. Nori, and L. Yang, Parity-time symmetry and exceptional points in photonics, *Nat. Mater.* **18**, 783 (2019).

[15] J. Wiersig, Review of exceptional point-based sensors, *Photon. Res.* **8**, 1457 (2020).

[16] E. J. Bergholtz, J. C. Budich, and F. K. Kunst, Exceptional topology of non-Hermitian systems, *Rev. Mod. Phys.* **93**, 015005 (2021).

[17] H. Zhang, T. Liu, Z. Xiang, K. Xu, H. Fan, and D. Zheng, Topological Eigenvalue Braiding and Quantum State Transfer Near a Third-Order Exceptional Point, *PRX Quantum* **6**, 020328 (2025).

[18] W. D. Heiss, The physics of exceptional points, *J. Phys. A: Math. Theor.* **45**, 444016 (2012).

[19] J. Schnabel, H. Cartarius, J. Main, G. Wunner, and W. D. Heiss,  $\mathcal{PT}$ -symmetric waveguide system with evidence of a third-order exceptional point, *Phys. Rev. A* **95**, 053868 (2017).

[20] S. Chakraborty, and A. K. Sarma, Delayed sudden death of entanglement at exceptional points, *Phys. Rev. A* **100**, 063846 (2019).

[21] A. Laha, D. Beniwal, S. Dey, A. Biswas, and S. Ghosh, Third-order exceptional point and successive switching among three states in an optical microcavity, *Phys. Rev. A* **101**, 063829 (2020).

[22] S. Ramezanpour, and A. Bogdanov, Tuning exceptional points with Kerr nonlinearity, *Phys. Rev. A* **103**, 043510 (2021).

[23] I. Mandal, and E. J. Bergholtz, Symmetry and Higher-Order Exceptional Points, *Phys. Rev. Lett.* **127**, 186601 (2021).

[24] Z. Lin, H. Ramezani, T. Eichelkraut, T. Kottos, H. Cao, and D. N. Christodoulides, Unidirectional Invisibility Induced by  $\mathcal{PT}$ -Symmetric Periodic Structures, *Phys. Rev. Lett.* **106**, 213901 (2011).

[25] B. Peng, Ş. K. Özdemir, F. Lei, F. Monifi, M. Gianfreda, G. L. Long, S. Fan, F. Nori, C. M. Bender, and L. Yang, Parity-time-symmetric whispering-gallery microcavities, *Nat. Phys.*

**10**, 394 (2014).

[26] S. Assawaworrarit, X. Yu, and S. Fan, Robust wireless power transfer using a nonlinear parity-time-symmetric circuit, *Nature* **546**, 387 (2017).

[27] X. Hao, K. Yin, J. Zou, R. Wang, Y. Huang, X. Ma, and T. Dong, Frequency-Stable Robust Wireless Power Transfer Based on High-Order Pseudo-Hermitian Physics, *Phys. Rev. Lett.* **130**, 077202 (2023).

[28] J. Doppler, A. A. Mailybaev, J. Böhm, U. Kuhl, A. Girschik, F. Libisch, T. J. Milburn, P. Rabl, N. Moiseyev, and S. Rotter, Dynamically encircling an exceptional point for asymmetric mode switching, *Nature* **537**, 76 (2016).

[29] H. Xu, D. Mason, L. Jiang, and J. G. E. Harris, Topological energy transfer in an optomechanical system with exceptional points, *Nature* **537**, 80 (2016).

[30] Z. Lin, A. Pick, M. Lončar, and A. W. Rodriguez, Enhanced Spontaneous Emission at Third-Order Dirac Exceptional Points in Inverse-Designed Photonic Crystals, *Phys. Rev. Lett.* **117**, 107402 (2016).

[31] S. Longhi and L. Feng, Unidirectional lasing in semiconductor microring lasers at an exceptional point, *Photon. Res.* **5**, B1 (2017).

[32] H. Zhou, C. Peng, Y. Yoon, C. W. Hsu, K. A. Nelson, L. Fu, J. D. Joannopoulos, M. Soljačić, and B. Zhen, Observation of bulk Fermi arc and polarization half charge from paired exceptional points, *Science* **359**, 1009 (2018).

[33] J. Wiersig, Enhancing the Sensitivity of Frequency and Energy Splitting Detection by Using Exceptional Points: Application to Microcavity Sensors for Single-Particle Detection, *Phys. Rev. Lett.* **112**, 203901 (2014).

[34] W. Chen, S. K. Özdemir, G. Zhao, J. Wiersig, and L. Yang, Exceptional points enhance sensing in an optical microcavity, *Nature* **548**, 192 (2017).

[35] G. Q. Zhang, Z. Chen, D. Xu, N. Shammah, M. Liao, T. F. Li, L. Tong, S. Y. Zhu, F. Nori, and J. Q. You, Exceptional point and cross-relaxation effect in a hybrid quantum system, *PRX Quantum* **2**, 020307 (2021).

[36] Z. P. Liu, J. Zhang, S. K. Özdemir, B. Peng, H. Jing, X. Y. Lü, C. W. Li, L. Yang, F. Nori, and Y. X. Liu, Metrology with  $\mathcal{PT}$ -Symmetric Cavities: Enhanced Sensitivity near the  $\mathcal{PT}$ -Phase Transition, *Phys. Rev. Lett.* **117**, 110802 (2016).

[37] H. Hodaei, A. U. Hassan, S. Wittek, H. Garcia-Gracia, R. El-Ganainy, D. N. Christodoulides, and M. Khajavikhan, Enhanced sensitivity at higher-order exceptional points, *Nature* **548**, 187 (2017).

[38] L. Feng, Z. J. Wong, R. M. Ma, Y. Wang, and X. Zhang, Single-mode laser by parity-time symmetry breaking, *Science* **346**, 972 (2014).

[39] H. Hodaei, M. A. Miri, M. Heinrich, D. N. Christodoulides, and M. Khajavikhan, Parity-time-symmetric microring lasers, *Science* **346**, 975 (2014).

[40] Y. Sun, W. Tan, H. Li, J. Li, and H. Chen, Experimental Demonstration of a Coherent Perfect Absorber with  $\mathcal{PT}$  Phase Transition, *Phys. Rev. Lett.* **112**, 143903 (2014).

[41] D. Zhang, X. Q. Luo, Y. P. Wang, T. F. Li, and J. Q. You, Observation of the exceptional point in cavity magnon-polaritons, *Nat. Commun.* **8**, 1368 (2017).

[42] C. Wang, W. R. Sweeney, A. D. Stone, and L. Yang, Coherent perfect absorption at an exceptional point, *Science* **373**, 1261 (2021).

[43] C. Wang, X. Jiang, G. Zhao, M. Zhang, C. W. Hsu, B. Peng, A. D. Stone, L. Jiang, and L. Yang, Electromagnetically induced transparency at a chiral exceptional point, *Nat. Phys.* **16**, 334 (2020).

[44] Z. Z. Li, W. Chen, M. Abbasi, K. W. Murch, and K. B. Whaley, Speeding up entanglement generation by proximity to higher-order exceptional points, *Phys. Rev. Lett.* **131**, 100202 (2023).

[45] K. Ding, G. Ma, M. Xiao, Z. Q. Zhang, and C. T. Chan, Emergence, Coalescence, and Topological Properties of Multiple Exceptional Points and Their Experimental Realization, *Phys. Rev. X* **6**, 021007 (2016).

[46] A. Mostafazadeh, Pseudo-Hermiticity versus  $\mathcal{PT}$  symmetry: The necessary condition for the reality of the spectrum of a non-Hermitian Hamiltonian, *J. Math. Phys.* **43**, 205 (2002).

[47] A. Mostafazadeh, Pseudo-Hermiticity versus  $\mathcal{PT}$  symmetry II: A complete characterization of non-Hermitian Hamiltonians with a real spectrum, *J. Math. Phys.* **43**, 2814 (2002).

[48] A. Mostafazadeh, Pseudo-Hermiticity versus  $\mathcal{PT}$  symmetry III: Equivalence of pseudo-Hermiticity and the presence of antilinear symmetries, *J. Math. Phys.* **43**, 3944 (2002).

[49] T. Deguchi and P. K. Ghosh, Quantum phase transition in a pseudo-Hermitian Dicke model, *Phys. Rev. E* **80**, 021107 (2009).

[50] T. Deguchi, P. K. Ghosh, and K. Kudo, Level statistics of a pseudo-Hermitian Dicke model, *Phys. Rev. E* **80**, 026213 (2009).

[51] H. Z. Shen, X. Q. Shao, G. C. Wang, X. L. Zhao, and X. X. Yi, Quantum phase transition in a coupled two-level system embedded in anisotropic three-dimensional photonic crystals, *Phys. Rev. E* **93**, 012107 (2016).

[52] L. S. Simeonov and N. V. Vitanov, Dynamical invariants for pseudo-Hermitian Hamiltonians, *Phys. Rev. A* **93**, 012123 (2016).

[53] V. V. Konotop, J. Yang, and D. A. Zezyulin, Nonlinear waves in  $\mathcal{PT}$ -symmetric systems, *Rev. Mod. Phys.* **88**, 035002 (2016).

[54] X. Y. Lü, H. Jing, J. Y. Ma, and Y. Wu,  $\mathcal{PT}$ -Symmetry Breaking Chaos in Optomechanics, *Phys. Rev. Lett.* **114**, 253601 (2015).

[55] L. Chang, X. Jiang, S. Hua, C. Yang, J. Wen, L. Jiang, G. Li, G. Wang, and M. Xiao, Parity-time symmetry and variable optical isolation in active-passive-coupled microresonators, *Nat. Photonics* **8**, 524 (2014).

[56] Y. P. Gao, C. Cao, T. J. Wang, Y. Zhang, and C. Wang, Cavity-mediated coupling of phonons and magnons, *Phys. Rev. A* **96**, 023826 (2017).

[57] G. Q. Zhang and J. Q. You, Higher-order exceptional point in a cavity magnonics system, *Phys. Rev. B* **99**, 054404 (2019).

[58] G. Q. Zhang, Y. Wang, and W. Xiong, Detection sensitivity enhancement of magnon Kerr nonlinearity in cavity magnonics induced by coherent perfect absorption, *Phys. Rev. B* **107**, 064417 (2023).

[59] Y. D. Hu, Y. P. Wang, R. C. Shen, Z. Q. Wang, W. J. Wu, and J. Q. You, Synthetically enhanced sensitivity using higher-order exceptional point and coherent perfect absorption, *arXiv:2401.01613*.

[60] W. Xiong, Z. Li, Y. Song, J. Chen, G. Q. Zhang, and M. Wang, Higher-order exceptional point in a pseudo-Hermitian cavity optomechanical system, *Phys. Rev. A* **104**, 063508 (2021).

[61] W. Xiong, Z. Li, G. Q. Zhang, M. Wang, H. C. Li, X. Q. Luo, and J. Chen, Higher-order exceptional point in a blue-detuned non-Hermitian cavity optomechanical system, *Phys. Rev. A* **106**, 033518 (2022).

[62] K. Yin, X. Hao, Y. Huang, J. Zou, X. Ma, and T. Dong, High-Order Exceptional Points in Pseudo-Hermitian Radio-Frequency Circuits, *Phys. Rev. Applied* **20**, L021003 (2023).

[63] M. A. Nielsen and I. L. Chuang, *Quantum Computation and Quantum Information* (Cambridge University Press, Cambridge, 2000).

[64] H. P. Breuer and F. Petruccione, *The Theory of Open Quantum Systems* (Oxford University Press, Oxford, UK, 2002).

[65] H. P. Breuer, E. M. Laine, J. Piilo, and B. Vacchini, Colloquium: Non-Markovian dynamics in open quantum systems, *Rev. Mod. Phys.* **88**, 021002 (2016).

[66] I. de Vega and D. Alonso, Dynamics of non-Markovian open quantum systems, *Rev. Mod. Phys.* **89**, 015001 (2017).

[67] P. Figueroa-Romero, K. Modi, R. J. Harris, T. M. Stace, and M. H. Hsieh, Randomized Benchmarking for Non-Markovian Noise, *PRX Quantum* **2**, 040351 (2021).

[68] F. Caruso, V. Giovannetti, C. Lupo, and S. Mancini, Quantum channels and memory effects, *Rev. Mod. Phys.* **86**, 1203 (2014).

[69] C. W. Gardiner and P. Zoller, *Quantum Noise* (Springer-Verlag, Berlin, 2000).

[70] J. G. Li, J. Zou, and B. Shao, Non-Markovianity of the damped Jaynes-Cummings model with detuning, *Phys. Rev. A* **81**, 062124 (2010).

[71] G. A. L. White, F. A. Pollock, L. C. L. Hollenberg, K. Modi, and C. D. Hill, Non-Markovian Quantum Process Tomography, *PRX Quantum* **3**, 020344 (2022).

[72] S. Milz, and K. Modi, Quantum Stochastic Processes and Quantum non-Markovian Phenomena, *PRX Quantum* **2**, 030201 (2021).

[73] D. Gribben, D. M. Rouse, J. Iles-Smith, A. Strathearn, H. Maguire, P. Kirton, A. Nazir, E. M. Gauger, and B. W. Lovett, Exact Dynamics of Nonadditive Environments in Non-Markovian Open Quantum Systems, *PRX Quantum* **3**, 010321 (2022).

[74] Z. Mann, N. Cao, R. Laflamme, and S. Zhou, Quantum Error-Corrected Non-Markovian Metrology, *PRX Quantum* **6**, 030321 (2025).

[75] L. Diósi, Non-Markovian open quantum systems: Input-output fields, memory, and monitoring, *Phys. Rev. A* **85**, 034101 (2012).

[76] H. Z. Shen, C. Shang, Y. H. Zhou, and X. X. Yi, Unconventional single-photon blockade in non-Markovian systems, *Phys. Rev. A* **98**, 023856 (2018).

[77] V. Link, K. Müller, R. G. Lena, K. Luoma, F. Damanet, W. T. Strunz, and A. J. Daley, Non-Markovian quantum dynamics in strongly coupled multimode cavities conditioned on continuous measurement, *PRX Quantum* **3**, 020348 (2022).

[78] U. Hoepppe, C. Wolff, J. Küchenmeister, J. Niegemann, M. Drescher, H. Benner, and K. Busch, Direct Observation of Non-Markovian Radiation Dynamics in 3D Bulk Photonic Crystals, *Phys. Rev. Lett.* **108**, 043603 (2012).

[79] J. I. Costa-Filho, R. B. B. Lima, R. R. Paiva, P. M. Soares, W. A. M. Morgado, R. L. Franco, and D. O. Soares-Pinto, Enabling quantum non-Markovian dynamics by injection of classical colored noise, *Phys. Rev. A* **95**, 052126 (2017).

[80] S. Longhi, Non-Markovian decay and lasing condition in an optical microcavity coupled to a structured reservoir, *Phys. Rev. A* **74**, 063826 (2006).

[81] H. T. Tan and W. M. Zhang, Non-Markovian dynamics of an open quantum system with initial system-reservoir correlations: A nanocavity coupled to a coupled-resonator optical waveguide, *Phys. Rev. A* **83**, 032102 (2011).

[82] H. Z. Shen, J. F. Yang, and X. X. Yi, Unconventional photon blockade with non-Markovian effects in driven dissipative coupled cavities, *Phys. Rev. A* **109**, 043714 (2024).

[83] J. D. Lin, P. C. Kuo, N. Lambert, A. Miranowicz, F. Nori, and Y. N. Chen, Non-Markovian Quantum Exceptional Points, *Nat. Commun.* **16**, 1289 (2025).

[84] A. Wilkey, Y. N. Joglekar, and G. Vemuri, Exceptional Points in a Non-Markovian Anti-Parity-Time Symmetric System, *Photonics* **10**, 1299 (2023).

[85] G. Mouloudakis and P. Lambropoulos, Coalescence of non-Markovian dissipation, quantum Zeno effect, and non-Hermitian physics in a simple realistic quantum system, *Phys. Rev. A* **106**, 053709 (2022).

[86] S. Garmon, G. Ordóñez, and N. Hatano, Anomalous-order exceptional point and non-Markovian Purcell effect at threshold in one-dimensional continuum systems, *Phys. Rev. Research* **3**, 033029 (2021).

[87] J. F. Yang and H. Z. Shen, Exceptional-point-engineered dispersive readout of a driven three-level atom weakly interacting with coupled cavities in non-Markovian environments, *Phys. Rev. A* **109**, 053712 (2024).

[88] B. H. Liu, L. Li, Y. F. Huang, C. F. Li, G. C. Guo, E. M. Laine, H. P. Breuer, and J. Piilo, Experimental control of the transition from Markovian to non-Markovian dynamics of open quantum systems, *Nat. Phys.* **7**, 931 (2011).

[89] S. J. Xiong, Q. Hu, Z. Sun, L. Yu, Q. Su, J. M. Liu, and C. P. Yang, Non-Markovianity in experimentally simulated quantum channels: Role of counterrotating-wave terms, *Phys. Rev. A* **100**, 032101 (2019).

[90] S. Cialdi, C. Benedetti, D. Tamascelli, S. Olivares, M. G. A. Paris, and B. Vacchini, Experimental investigation of the effect of classical noise on quantum non-Markovian dynamics, *Phys. Rev. A* **100**, 052104 (2019).

[91] D. Khurana, B. K. Agarwalla, and T. S. Mahesh, Experimental emulation of quantum non-Markovian dynamics and coherence protection in the presence of information backflow, *Phys. Rev. A* **99**, 022107 (2019).

[92] K. H. Madsen, S. Ates, T. Lund-Hansen, A. Löffler, S. Reitzenstein, A. Forchel, and P. Lodahl, Observation of Non-Markovian Dynamics of a Single Quantum Dot in a Micropillar Cavity, *Phys. Rev. Lett.* **106**, 233601 (2011).

[93] Y. Guo, P. Taranto, B. H. Liu, X. M. Hu, Y. F. Huang, C. F. Li, and G. C. Guo, Experimental Demonstration of Instrument-Specific Quantum Memory Effects and Non-Markovian Process Recovery for Common-Cause Processes, *Phys. Rev. Lett.* **126**, 230401 (2021).

[94] B. W. Li, Q. X. Mei, Y. K. Wu, M. L. Cai, Y. Wang, L. Yao, Z. C. Zhou, and L. M. Duan, Observation of Non-Markovian Spin Dynamics in a Jaynes-Cummings-Hubbard Model Using a Trapped-Ion Quantum Simulator, *Phys. Rev. Lett.* **129**, 140501 (2022).

[95] J. S. Xu, C. F. Li, C. J. Zhang, X. Y. Xu, Y. S. Zhang, and G. C. Guo, Experimental investigation of the non-Markovian dynamics of classical and quantum correlations, *Phys. Rev. A* **82**, 042328 (2010).

[96] S. A. Uriri, F. Wudarski, I. Sinayskiy, F. Petruccione, and M. S. Tame, Experimental investigation of Markovian and non-Markovian channel addition, *Phys. Rev. A* **101**, 052107 (2020).

[97] M. H. Anderson, G. Vemuri, J. Cooper, P. Zoller, and S. J. Smith, Experimental study of absorption and gain by two-level atoms in a time-delayed non-Markovian optical field, *Phys. Rev. A* **47**, 3202 (1993).

[98] Z. D. Liu, Y. N. Sun, B. H. Liu, C. F. Li, G. C. Guo, S. Hamedani Raja, H. Lyra, and J. Piilo, Experimental realization of high-fidelity teleportation via a non-Markovian open quantum system, *Phys. Rev. A* **102**, 062208 (2020).

[99] S. Gröblacher, A. Trubarov, N. Prigge, G. D. Cole, M. Aspelmeyer, and J. Eisert, Observation of non-Markovian micromechanical Brownian motion, *Nat. Commun.* **6**, 7606 (2015).

[100] H. Z. Shen, S. Xu, H. T. Cui, and X. X. Yi, Non-Markovian dynamics of a system of two-level atoms coupled to a structured environment, *Phys. Rev. A* **99**, 032101 (2019).

[101] L. Xin, S. Xu, X. X. Yi, and H. Z. Shen, Tunable non-Markovian dynamics with a three-level atom mediated by the classical laser in a semi-infinite photonic waveguide, *Phys. Rev. A* **105**, 053706 (2022).

[102] H. Z. Shen, Q. Wang, and X. X. Yi, Dispersive readout with non-Markovian environments, *Phys. Rev. A* **105**, 023707 (2022).

[103] S. Lorenzo, F. Plastina, and M. Paternostro, Geometrical characterization of non-Markovianity, *Phys. Rev. A* **88**, 020102(R) (2013).

[104] A. Rivas, S. F. Huelga, and M. B. Plenio, Entanglement and non-Markovianity of quantum evolutions, *Phys. Rev. Lett.* **105**, 050403 (2010).

[105] S. Luo, S. Fu, and H. Song, Quantifying non-Markovianity via correlations, *Phys. Rev. A* **86**, 044101 (2012).

[106] M. M. Wolf, J. Eisert, T. S. Cubitt, and J. I. Cirac, Assessing non-Markovian quantum dynamics, *Phys. Rev. Lett.* **101**, 150402 (2008).

[107] X. M. Lu, X. Wang, and C. P. Sun, Quantum Fisher information flow and non-Markovian processes of open systems, *Phys. Rev. A* **82**, 042103 (2010).

[108] D. Chruściński and S. Maniscalco, Degree of non-Markovianity of quantum evolution, *Phys. Rev. Lett.* **112**, 120404 (2014).

[109] Z. Li, X. Li, and X. Zhong, High-order exceptional point in a nanofiber cavity quantum electrodynamics system, *arXiv:2201.03768*.

[110] J. Kullig, C. H. Yi, M. Hentschel, and J. Wiersig, Exceptional points of third-order in a layered optical microdisk cavity, *New J. Phys.* **20**, 083016 (2018).

[111] H. Jing, Ş. K. Özdemir, H. Lü, and F. Nori, High-order exceptional points in optomechanics, *Sci. Rep.* **7**, 3386 (2017).

[112] N. Habler and J. Scheuer, Higher-order exceptional points: A route for flat-top optical filters, *Phys. Rev. A* **101**, 043828 (2020).

[113] A. Sahoo and A. K. Sarma, Two-way enhancement of sensitivity by tailoring higher-order exceptional points, *Phys. Rev. A* **106**, 023508 (2022).

[114] A. Novitsky, F. Morozko, D. Gao, L. Gao, A. Karabchevsky, and D. V. Novitsky, Resonance energy transfer near higher-order exceptional points of non-hermitian hamiltonians, *Phys. Rev. B* **106**, 195410 (2022).

[115] A. Montag and F. K. Kunst, Symmetry-induced higher-order exceptional points in two dimensions, *Phys. Rev. Research* **6**, 023205 (2024).

[116] Y. Zhang, S. Xia, X. Zhao, L. Qin, X. Feng, W. Qi, Y. Jiang, H. Lu, D. Song, L. Tang, Z. Zhu, W. Liu, and Y. Liu, Symmetry-protected third-order exceptional points in staggered flatband rhombic lattices, *Photonics Res.* **11**, 225 (2023).

[117] L. Crippa, J. C. Budich, and G. Sangiovanni, Fourth-order exceptional points in correlated quantum many-body systems, *Phys. Rev. B* **104**, L121109 (2021).

[118] S. Bhattacherjee, H. K. Gandhi, A. Laha, and S. Ghosh, Higher-order topological degeneracies and progress towards unique successive state switching in a four-level open system, *Phys. Rev. A* **100**, 062124 (2019).

[119] L. Jin, Parity-time-symmetric coupled asymmetric dimers, *Phys. Rev. A* **97**, 012121 (2018).

[120] M. A. K. Othman, V. Galdi, and F. Capolino, Exceptional points of degeneracy and  $\mathcal{PT}$  symmetry in photonic coupled chains of scatterers, *Phys. Rev. B* **95**, 104305 (2017).

[121] S. Dey, A. Laha, and S. Ghosh, Exotic light dynamics around a fourth order exceptional point, *arXiv:2008.07903v1*.

[122] I. I. Arkhipov, F. Minganti, A. Miranowicz, and F. Nori, Generating high-order quantum exceptional points in synthetic dimensions, *Phys. Rev. A* **104**, 012205 (2021).

[123] X. Zhou, S. K. Gupta, Z. Huang, Z. Yan, P. Zhan, Z. Chen, M. Lu, and Z. Wang, Optical lattices with higher-order exceptional points by non-Hermitian coupling, *Appl. Phys. Lett.* **113**, 101108 (2018).

[124] X. Shen, K. Pan, X. Wang, H. Jiang, and X. Zhou, Gain and loss induced higher-order exceptional points in a non-Hermitian electrical circuit, *J. Phys. D: Appl. Phys.* **57**, 065102 (2024).

[125] D. Kaltsas, I. Komis, and K. G. Makris, Higher order exceptional points in infinite lattices, *Opt. Letters* **47**, 4447 (2022).

[126] Q. Zhong, J. Kou, Ş. K. Özdemir, and R. El-Ganainy, Hierarchical Construction of Higher-Order Exceptional Points, *Phys. Rev. Lett.* **125**, 203602 (2020).

[127] K. Bai, J. Z. Li, T. R. Liu, L. Fang, D. Wan, and M. Xiao, Non-linear Exceptional Points with a Complete Basis in Dynamics, *Phys. Rev. Lett.* **130**, 266901 (2023).

[128] L. Pan, S. Chen, and X. Cui, Interacting non-Hermitian ultracold atoms in a harmonic trap: Two-body exact solution and a high-order exceptional point, *Phys. Rev. A* **99**, 063616 (2019).

[129] S. M. Zhang, X. Z. Zhang, L. Jin, and Z. Song, High-order exceptional points in supersymmetric arrays, *Phys. Rev. A* **101**, 033820 (2020).

[130] Z. Xiao, H. Li, T. Kottos, and A. Alù, Enhanced Sensing and Nondegraded Thermal Noise Performance Based on  $\mathcal{PT}$ -Symmetric Electronic Circuits with a Sixth-Order Exceptional Point, *Phys. Rev. Lett.* **123**, 213901 (2019).

[131] J. Kullig, D. Grom, S. Klembt, and J. Wiersig, Higher-order exceptional points in waveguide-coupled microcavities: perturbation induced frequency splitting and mode patterns, *Photonics Res.* **11**, A54 (2023).

[132] A. Almanakly, B. Yankelevich, M. Hays, B. Kannan, R. Assouly, A. Greene, M. Gingras, B. M. Niedzielski, H. Stickler, M. E. Schwartz, K. Serniak, J. I. J. Wang, T. P. Orlando, S. Gustavsson, J. A. Grover, and W. D. Oliver, Deterministic remote entanglement using a chiral quantum interconnect, *Nat. Phys.* **21**, 825 (2025).

[133] W. Nie, T. Shi, Y. X. Liu, and F. Nori, Non-Hermitian Waveguide Cavity QED with Tunable Atomic Mirrors, *Phys. Rev. Lett.* **131**, 103602 (2023).

[134] B. Kannan, A. Almanakly, Y. Sung, A. Di Paolo, D. A. Rower, J. Braumüller, A. Melville, B. M. Niedzielski, A. Karamlou, K. Serniak, A. Vepsäläinen, M. E. Schwartz, J. L. Yoder, R. Winik, J. I. J. Wang, T. P. Orlando, S. Gustavsson, J. A. Grover, and W. D. Oliver, On-demand directional microwave photon emission using waveguide quantum electrodynamics, *Nat. Phys.* **19**, 394 (2023).

[135] G. Q. Zhang, Z. Chen, and J. Q. You, Experimentally accessible quantum phase transition in a non-Hermitian Tavis-Cummings model engineered with two drive fields, *Phys. Rev. A* **102**, 032202 (2020).

[136] X. Gu, A. F. Kockum, A. Miranowicz, Y. X. Liu, and F. Nori, Microwave photonics with superconducting quantum circuits, *Phys. Rep.* **718-719**, 1 (2017).

[137] A. Baust, E. Hoffmann, M. Haeberlein, M. J. Schwarz, P. Eder, J. Goetz, F. Wulschner, E. Xie, L. Zhong, F. Quijandría, B. Peropadre, D. Zueco, J. J. G. Ripoll, E. Solano, K. Fedorov, E. P. Menzel, F. Deppe, A. Marx, and R. Gross, Tunable and switchable coupling between two superconducting resonators, *Phys. Rev. B* **91**, 014515 (2015).

[138] H. L. Zhang, P. R. Han, F. Wu, W. Ning, Z. B. Yang, and S. B. Zheng, Experimental observation of non-Markovian quantum exceptional points, arXiv: 2503.06977.

[139] G. Q. Qin, R. R. Xie, H. Zhang, Y. Q. Hu, M. Wang, G. Q. Li, H. Xu, F. Lei, D. Ruan, and G. L. Long, Experimental Realization of Sensitivity Enhancement and Suppression with Exceptional Surfaces, *Laser Photon. Rev.* **15**, 2000569 (2021).

[140] W. Li, Y. Zhou, P. Han, X. Chang, S. Jiang, A. Huang, H. Zhang, and Z. Xiao, Exceptional-surface-enhanced rotation sensing with robustness in a whispering-gallery-mode microresonator, *Phys. Rev. A* **104**, 033505 (2021).

[141] S. Jiang, J. Li, Z. Li, Z. Li, W. Li, X. Huang, H. Zhang, G. Zhang, A. Huang, and Z. Xiao, Experimental realization of exceptional surfaces enhanced displacement sensing with robustness, *Appl. Phys. Lett.* **123**, 201106 (2023).

[142] Q. Zhong, A. Hashemi, S. K. Özdemir, and R. El-Ganainy, Control of spontaneous emission dynamics in microcavities with chiral exceptional surfaces, *Phys. Rev. Research* **3**, 013220 (2021).

[143] S. Soleymani, Q. Zhong, M. Mokim, S. Rotter, R. El-Ganainy, and S. K. Özdemir, Chiral and degenerate perfect absorption on exceptional surfaces, *Nat. Commun.* **13**, 599 (2022).

[144] W. Tang, K. Ding, and G. Ma, Realization and topological properties of third-order exceptional lines embedded in exceptional surfaces, *Nat. Commun.* **14**, 6660 (2023).

[145] H. Jia, R. Y. Zhang, J. Hu, Y. Xiao, S. Zhang, Y. Zhu, and C. T. Chan, Topological classification for intersection singularities of exceptional surfaces in pseudo-Hermitian systems, *Commun. Phys.* **6**, 293 (2023).

[146] M. Stålhammar and E. J. Bergholtz, Classification of exceptional nodal topologies protected by  $\mathcal{PT}$  symmetry, *Phys. Rev. B* **104**, L201104 (2021).

[147] L. Chen, W. Wu, F. Huang, Y. Chen, G. S. Liu, Y. Luo, and Z. Chen, Chaotic dynamics on exceptional surfaces, *Phys. Rev. A* **105**, L031501 (2022).

[148] Q. Zhong, S. K. Özdemir, A. Eisfeld, A. Metelmann, and R. El-Ganainy, Exceptional Point-Based Optical Amplifiers, *Phys. Rev. Applied* **13**, 014070 (2020).

[149] H. Z. Shen, D. X. Li, and X. X. Yi, Non-Markovian linear response theory for quantum open systems and its applications, *Phys. Rev. E* **95**, 012156 (2017).

[150] G. E. Uhlenbeck and L. S. Ornstein, On the theory of the Brownian motion, *Phys. Rev.* **36**, 823 (1930).

[151] D. F. Walls and G. J. Milburn, *Quantum Optics* (Springer, Berlin, 2nd Edition, 2008).

[152] M. O. Scully and M. S. Zubairy, *Quantum Optics* (Cambridge University Press, Cambridge, 1997).

[153] C. Uchiyama, M. Aihara, M. Saeki, and S. Miyashita, Master equation approach to line shape in dissipative systems, *Phys. Rev. E* **80**, 021128 (2009).

[154] H. Z. Shen, M. Qin, X. Q. Shao, and X. X. Yi, General response formula and application to topological insulator in quantum open system, *Phys. Rev. E* **92**, 052122 (2015).

[155] K. Tschernig, K. Busch, D. N. Christodoulides, and A. Perez-Leija, Branching high-order exceptional points in non-Hermitian optical systems, *Laser Photon. Rev.* **16**, 2100707 (2022).

[156] H. Z. Shen, D. X. Li, S. L. Su, Y. H. Zhou, and X. X. Yi, Exact non-Markovian dynamics of qubits coupled to two interacting environments, *Phys. Rev. A* **96**, 033805 (2017).

[157] H. Z. Shen, S. L. Su, Y. H. Zhou, and X. X. Yi, Non-Markovian quantum Brownian motion in one dimension in electric fields, *Phys. Rev. A* **97**, 042121 (2018).

[158] H. Z. Shen, Q. Wang, J. Wang, and X. X. Yi, Nonreciprocal unconventional photon blockade in a driven dissipative cavity with parametric amplification, *Phys. Rev. A* **101**, 013826 (2020).

[159] Q. T. Xie, S. Cui, J. P. Cao, L. Amico, and H. Fan, Anisotropic Rabi model, *Phys. Rev. X* **4**, 021046 (2014).

[160] X. Y. Chen, L. Duan, D. Braak, and Q. H. Chen, Multiple ground-state instabilities in the anisotropic quantum Rabi model, *Phys. Rev. A* **103**, 043708 (2021).

[161] Q. Ai, Y. Li, H. Zheng, and C. P. Sun, Quantum anti-Zeno effect without rotating wave approximation, *Phys. Rev. A* **81**, 042116 (2010).

[162] Z. Lü and H. Zheng, Quantum dynamics of the dissipative two-state system coupled with a sub-Ohmic bath, *Phys. Rev. B* **75**, 054302 (2007).

[163] W. Alford, L. P. Bettmann, and G. T. Landi, Subtleties in the pseudomodes formalism, arXiv: 2509.16377.

[164] M. W. Jack and J. J. Hope, Resonance fluorescence in a band-gap material: Direct numerical simulation of non-Markovian evolution, *Phys. Rev. A* **63**, 043803 (2001).

[165] S. M. Barnett and P. M. Radmore, *Methods in Theoretical Quantum Optics* (Oxford University Press, Oxford, 1997).

[166] B. M. Garraway, Nonperturbative decay of an atomic system in a cavity, *Phys. Rev. A* **55**, 2290 (1997).

[167] B. M. Garraway, Decay of an atom coupled strongly to a reservoir, *Phys. Rev. A* **55**, 4636 (1997).

[168] Z. X. Man, N. B. An, and Y. J. Xia, Non-Markovianity of a two-level system transversally coupled to multiple bosonic reservoirs, *Phys. Rev. A* **90**, 062104 (2014).

[169] L. Mazzola, S. Maniscalco, J. Piilo, K. A. Suominen, and B. M. Garraway, Pseudomodes as an effective description of memory: Non-Markovian dynamics of two-state systems in structured reservoirs, *Phys. Rev. A* **80**, 012104 (2009).

[170] G. Pleasance and B. M. Garraway, Application of quantum Darwinism to a structured environment, *Phys. Rev. A* **96**, 062105 (2017).

[171] D. Tamascelli, A. Smirne, S. F. Huelga, and M. B. Plenio, Nonperturbative Treatment of non-Markovian Dynamics of Open Quantum Systems, *Phys. Rev. Lett.* **120**, 030402 (2018).